NRL Memorandum Report 5194

Additional Capabilities of the Unified Waves Model

J. M. WITTING

Laboratory for Computational Physics

September 29, 1983

NAVAL RESEARCH LABORATORY
Washington, D.C.

SECURITY CLASSIFICATION OF THIS PAGE (When Data Entered)

REPORT DOCUMENTATION PAGE		READ INSTRUCTIONS BEFORE COMPLETING FORM
1. REPORT NUMBER NRL Memorandum Report 5194	2. GOVT ACCESSION NO.	3. RECIPIENT'S CATALOG NUMBER
4. TITLE (and Subtitle) ADDITIONAL CAPABILITIES OF THE UNIFIED WAVES MODEL		5. TYPE OF REPORT & PERIOD COVERED Interim report on a continuing NRL problem. 6. PERFORMING ORG. REPORT NUMBER
7. AUTHOR(s) J. M. Witting		8. CONTRACT OR GRANT NUMBER(s)
9. PERFORMING ORGANIZATION NAME AND ADDRESS Naval Research Laboratory Washington, DC 20375		10. PROGRAM ELEMENT, PROJECT, TASK AREA & WORK UNIT NUMBERS 61153N; RR 032-04-03; 44-1868-03
11. CONTROLLING OFFICE NAME AND ADDRESS Office of Naval Research Arlington, VA 22217		12. REPORT DATE September 29, 1983 13. NUMBER OF PAGES 33
14. MONITORING AGENCY NAME & ADDRESS(if different from Controlling Office)		15. SECURITY CLASS. (of this report) UNCLASSIFIED 15a. DECLASSIFICATION/DOWNGRADING SCHEDULE
16. DISTRIBUTION STATEMENT (of this Report) Approved for public release; distribution unlimited.		
17. DISTRIBUTION STATEMENT (of the abstract entered in Block 20, if different from Report)		
18. SUPPLEMENTARY NOTES		
19. KEY WORDS (Continue on reverse side if necessary and identify by block number) Waterwaves Unified waves model Nonlinear Variable depth Wavemaker Steady nonuniform flow		

20. ABSTRACT (Continue on reverse side if necessary and identify by block number)

The initial report on the "unified waves model" describes a procedure to compute water wave propagation over long distances accurately, at low cost, and for a wide variety of physical situations (Witting, 1982). This report outlines recent developments that extend its capabilities. These involve: (1) inclusion of a variable depth, (2) addition of a wavemaker, and (3) the ability to send steady non-uniform flows through the computational domain. Examples of calculations employing the new capabilities are given.

DD FORM 1 JAN 73 1473 EDITION OF 1 NOV 65 IS OBSOLETE
S/N 0102-014-6601

SECURITY CLASSIFICATION OF THIS PAGE (When Data Entered)

CONTENTS

ADDITIONAL CAPABILITIES OF THE UNIFIED WAVES MODEL

1. Introduction

This brief report outlines developments that have been added to the unified waves model to extend its capability beyond that described by Witting (1982). These include: 1) inclusion of a variable depth, 2) addition of a wavemaker, and 3) inflow-outflow boundary conditions. Section 2 displays the new capabilities, and Section 3 provides details of the developments.

2. Displays of the New Capabilities

Figure 1 shows results for a run in a channel of variable depth, with a wave train generated by a wavemaker. Between $x = 80$ and $x = 160$ the channel shoals linearly from one depth to a depth ten times smaller. Distances are non-dimensionalized with the deep undisturbed depth being unity (Fig. 1a). The water is initially undisturbed (See lowermost trace of Fig. 1b). A wavemaker is then turned on to produce a moderate-amplitude wave traveling away from the rigid left-hand wall. Figure 1b is a coarse (every fourth grid point) snapshot of the wave elevation at the initial and 32 equally-spaced time levels. The spacing is such that a disturbance that travels at a speed $\sqrt{gh_\ell}$ (h_ℓ is the depth at the left) would show up along a $\pm 45^\circ$ angle in the figure. When the wave shoals it gets higher and thinner. Before the end of the run the numerical results show a wave with "higher

Manuscript approved May 26, 1983.

than breaking" slopes. The code crashed four time steps after the uppermost profile.*

The remainder of Fig. 1 gives details. Figures (1c-1j) show that the wavemaker is working satisfactorily. These are blown-up views of the 5th, 9th..., 33rd profiles of Fig 1b, for the leftmost 600 grid points (there are 1600 grid points in the computational box; $\Delta x = \Delta t = 1/8$ for this calculation). The wavemaker produces smooth waves. Details of the wavemaker will be given in Section 3B.

Figures (1k-1r) center attention on the next 600 grid points. The shoaling starts at grid point 640 and continues to grid point 1280. The 29th profile (Fig. 1q) is used for discussion. It is a continuation of Fig. 1i. The leftmost wave in Fig. 1q is a continuation of the steadily marching waves in Fig. 1i. The effects of shoaling are apparent in the rest of Fig. 1q. The waves get higher, and travel slower. They also become sharp-crested.

*The analysis and numerical methods conserve exactly those linear quantities that should be conserved from the exact prognostic equations resulting from applying the continuity and Euler equations to the situation (Witting and McDonald, 1982 derive the form used). These conserved quantities are the integrated mass and an integrated surface velocity. The model involves approximations, however, and physical energy is not conserved exactly, though the code is reversible, so that no "numerical" dissipation is introduced. The experience gained from running the model in a variety of problems is that energy is conserved rather precisely for physical conditions where waves are not breaking, but not so precisely for physical conditions where the waves would be breaking. Indeed, the model usually becomes rapidly unstable at wave amplitudes near (usually above) the breaking point. The inclusion of local dissipation to simulate breaking waves would be desireable both to improve the model and to stabilize it.

Figure 1r is taken 56 time steps later. The wave between 1050 and 1100 is very sharp-crested indeed. Four time steps later the instability that is seen starting here grew to floating-point overflow catastrophe.

Figures (1s-1z) concentrate on the uppermost 8 profiles of Figure 1b. Note changes in both vertical and horizontal scale from the previous figures. The last two (Figs. 1y-1z) show the sharp-crestedness.

Figures (1aa-1ee) center attention near grid point 1075, where the wave breaking eventually occurs, for the uppermost five profiles of Fig. 1b. The scales are set so that the profiles are not vertically exaggerated, and the location of the shoaling bottom is shown. As we proceed from Fig. 1aa through Fig. 1dd note the solitary-wave-like appearance, with increasing amplitude. The amplitude and maximum slopes of Fig. 1dd exceed those for breaking progressive waves. Fig. 1ee shows what is about to happen to the numerics when the model wave height is about twice that of the highest wave in water. Details of how the variable depth has been added to the unified waves model are described in Section 3A.

Figure 2a is a display of the inflow-outflow capability. A steady flow is directed from right to left in a channel of variable breadth that is narrower at the right than at the left. Consequently, the flow is decelerating from right to left. A wave packet initially centered at x=50, is designed to move to the right (but a little disturbance also moves to the left). Figure 2a shows the resulting fate of the packet (its caption summarizes what happens). As can be seen from the figure, the waves are blocked by the adverse currents. Linear theory predicts the blocking location to be at x=119.

The calculations for Fig. 2 differ from those of Fig. 1 and all those in Witting (1982) in that a "trapezoidal correction"is added at each time step. This procedure is slightly dissipative, suppressing an alternating grid point instability that is bothersome when steady currents run through the computational channel. Consequently, it is not possible to track the wave packet's energy with the data shown in Fig. 2. A successful effort has been made in subsequent calculations that suppress instabilities toward the right of $x=150$ but are dissipationless for $x<150$, over which all the action takes place. These run to longer times. Results agree with those of Figure 2. They show that the packet reflects no visible waves, and remains nearly stationary with its leading edge near $x=120$ (phases enter at the left and disappear at the right of this dispersive wave train). Amplitudes and slopes at the front of the train eventually exceed those of breaking waves, and so the physical situation would be that of deep-water whitecapping. It may be concluded that the fate of a wave packet encountering sufficiently strong adverse currents is to break.

Figures (2b-2i) are centered at the point at which the steady current gradients are near maximum. On display are blowups of the 5th, 9th,...,33rd (uppermost) curve of Fig. 2a. Note the decrease in wavelength, the increase in amplitude, and eventual sharp-crestedness of the waves in the center of the train. Some of the increase in amplitude is caused by the waves passing through a gradually narrower channel. The majority is due to wave-current interaction. Details of how the inflow-outflow capability has been added to the model are given in Section 3C.

3. Discussion of the New Capabilities

3A. Variable Depth

The analysis presented in Witting (1982) is valid for waves in channels of gradually varying breadth and depth. In the initial computer implementation, however, the depth was set to unity, and the "h" that appeared in the analysis was replaced by $1+\eta(x,t)$ To get the depth into the problem, it was necessary only to replace $1+\eta(x,t)$ with $h_o(x) + \eta(x,t)$, where $h_o(x)$ is the undisturbed depth normalized to a depth somewhere in the channel, x_o, say, where $h_o(x_o)=1$. The undisturbed depths $h_o(x)$ are supplied to the computer externally (by assigning a file and reading it). No difficulities were experienced in the course of adding the variable depth capability.

The $h_o(x)$ used in Fig. 1 is a set of three straight lines with intersections smoothed over a distance of approprimately $0.5\ h_o(x_o)$. No tests were performed to see whether unsmoothed variable depth channels would pose numerical problems.

3B. Wavemaker

A wavemaker was needed to be able to continuously deposit energy with known frequency and wavelength content into the channel, preferably near one end. Pumping water into and out of the channel from an end produced waves with ragged waveforms. An alternate procedure, pumping water without horizontal momentum into and out of the channel at several grid points near an end produces waveforms of the quality of those shown in Figs (1c-1j).

The procedure for designing the wavemaker employs linear water wave theory:

$$\frac{\partial \eta}{\partial t} + h_o \frac{\partial \bar{u}}{\partial x} = Q(x,t) \qquad (1)$$

$$\frac{\partial u_s}{\partial t} + g \frac{\partial \eta}{\partial x} = 0 \qquad (2)$$

where η is the elevation above still water level, $\bar{u}$ is the vertically averaged horizontal velocity, u_s is the horizontal component of surface velocity, $Q(x,t)$ is a mass source (the zero on the right side of (2) implies that no horizontal momentum is injected into the fluid). For linear sinusoidal waves one can show that

$$\bar{u} = u_s \tanh (kh_o)/kh_o. \qquad (3)$$

We want to find $Q(x,t)$ such that a nice wave comes out. We do this by writing the elevation as a function that behaves like a progressive wave as $x \to \infty$ and as a standing wave with antinode at $x=0$ at the wall where the velocity vanishes. We take a steady-state solution. For Fig. 1 the form chosen is:

$$\eta = \eta_o \{\cos \omega t \cos kx + \sin \omega t \sin kx \tanh \alpha x\} \qquad (4)$$

The next step is to evaluate u_s using (4) and (2). Then evaluate $\bar{u}$ from u_s using (3).

Finally, after algebra, (1) gives:

$$Q = 2\omega\eta_o \cos \omega t \operatorname{sech}^2 \alpha x \left\{\frac{\alpha}{k} \cos kx - \frac{\alpha^2}{k^2} \sin kx \tanh \alpha x\right\} \qquad (5)$$

In the numerical model source terms are inserted to permit mass injection at each time step of the form of (5), with k, η_o, and α beig inputted parameters, and ω being evaluated from the linear dispersion relation.

The data used to make the wave shown in Fig. 1 are:

$$kh_o = 1.0; \quad \frac{\eta_o}{h_o} = 0.1; \quad \alpha h_o = 0.1 \qquad (6)$$

After a short time the wave train has acquired some of the characteristics of (4) in its main body (note that (4) is a steady-state solution, and our wavemaker has Q=0 for time <0, and Q from Eq. (5) for t>0). In particular, the wave train has the expected wavelength and frequency. Its amplitude away from the wall exceeds that expected by tens of percent, however. This may be due to applying a linear, steady state analysis for waves that are nonlinear and initially transient. In any case, the wavemaker of (5) produces acceptably clean progressive waves of known frequency-wavelength content, which is good enough.

3C. Inflow-Outflow Conditions.

The goal of this development is to allow a steady current to flow through the computational channel; this differs from a frequently-required goal in computations, to let disturbances radiate out. The only coding change necessary in the running programs is to ensure that end wall boundary conditions are set to give a correct mass transport, surface velocity, and elevation that are appropriate for a steady, undisturbed flow. Consistency requires that if

$$q_s \equiv u_s + \eta' v_s \cong u_s = u_o \ , \tag{7}$$

$$\psi_s \equiv \int_0^h u\, b\, dy = u_o b h = u_o b\, [h_o + \eta_o(t)] \tag{8}$$

at the wall (or vice versa).

Providing suitable input files is a little more subtle. Assuming that volume fluxes into and out of the channel are the same, we can have a steady flow in a given geometry, but only if the initial surface elevations and velocities are set at precise values; otherwise long waves propagate. These long waves would bounce around the channel at speeds of the order of unity, and upset both numerical stability and interpretation. After some trial and error, a satisfactory way of handling the input files was found. A channel geometry can be selected and long wave theory used to give $\eta(x,t=0)$ that corresponds to a steady flow in this theory. From $\eta(x,t=0)$ and the known velocity at one wall one can compute exactly q_s $(x,t=0)$ for a steady flow from Bernoulli's Law. From η and q_s one then can recompute the channel geometry. The new geometry should differ only slightly from the original, but should keep the long wave steady.

The above procedure was used in part, for a channel of variable breadth (I have not yet tried it for a channel of variable depth). A smooth surface elevation was assumed for the steady flow of the form:

$$\eta(N) = -0.25\ (\Delta\eta)\ \tanh^2\ [\beta(N-800)\ +1] \qquad (9)$$

where N is the grid point number, $\Delta\eta$ is the magnitude of the depth change from end to end (=0.075 for Fig. 2), and β expresses how gradually the change occurs (=0.005 for Fig. 2). The velocity at the left was set to -0.100. With the profile of (9) it went to -0.400 at the right. The channel breadth that permits this is smoothly varying, between b=1.0 taken at the left to b=0.270 at the right. This channel breadth configuration and these steady flow conditions are shown in Fig. 3.

Onto the steady flow can be added either a wavemaker or a superposed initial disturbance well away from walls. The latter procedure was used for Fig. 2.

One may inquire what physical conditions match the endwall boundary conditions of the model. It appears that they are rigid walls for high-frequency waves, yet permit steady flow through them. A poraus, dense wall with high constant pressure head driving the steady flow seems to be a possible physical condition that corresponds this numerical implementation of the unified waves model.

References

Witting, J.M. (1982). A unified model for the evolution of nonlinear water waves; NRL Memorandum Report 5001 (December 30, 1982).

Witting, J.M. and B.E. McDonald (1982). A conservation-of-velocity law for inviscid fluids; NRL Memorandum Report 4977 (December 3, 1982).

Acknowledgments

This work was supported by the Coastal Sciences Group, Ocean Sciences Division, of the Office of Naval Research.

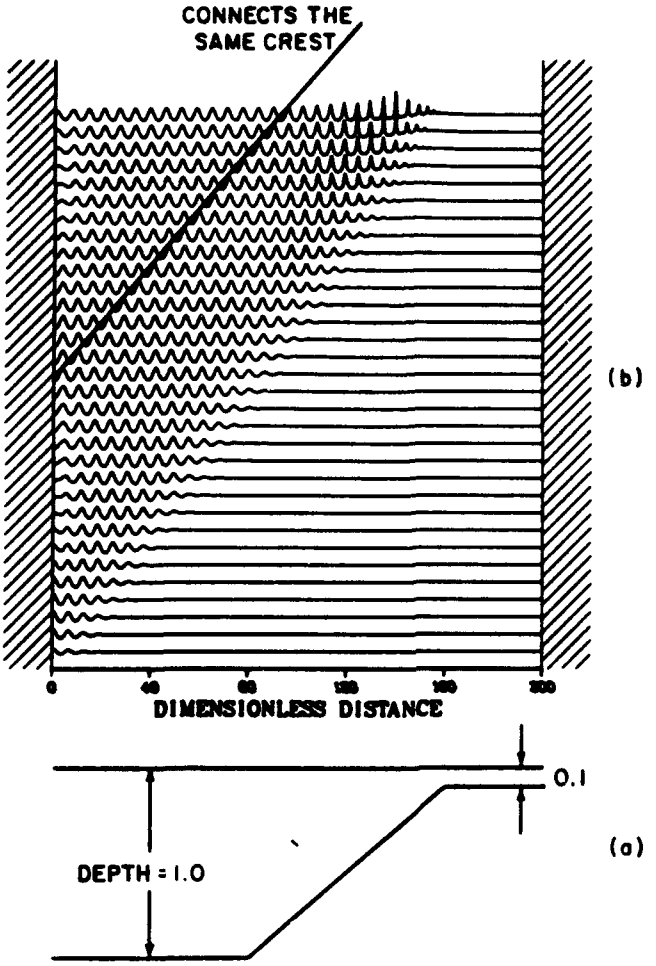

Fig. 1a and b — Waves generated by a wavemaker propagating through a channel of decreasing depth; (a) the geometry and (b) successive profiles of elevation, starting at the bottom. A wavemaker is turned on at t = 0 and makes waves at a fixed frequency such that the initial wavelength is $2\pi h_0$, h_0 being the undisturbed depth at the left. The spacing between successive profiles is scaled so that a feature that would travel at a speed $\sqrt{gh_0}$ would appear along a $\pm 45°$ line on the figure. The calculations are run with $\Delta x = \Delta t = 1/8$ for 1792 time steps (to t = 224) in a computational region of 1600 grid points (to x = 200).

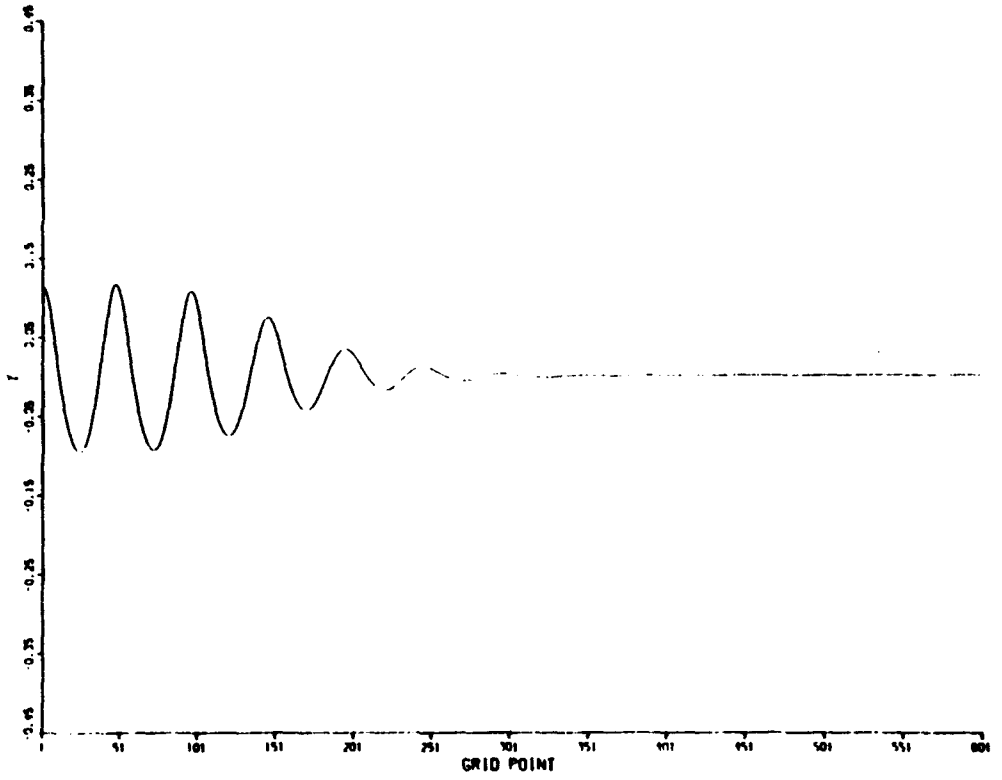

Fig. 1(c) — Details of the scene near the left wall at t = 28

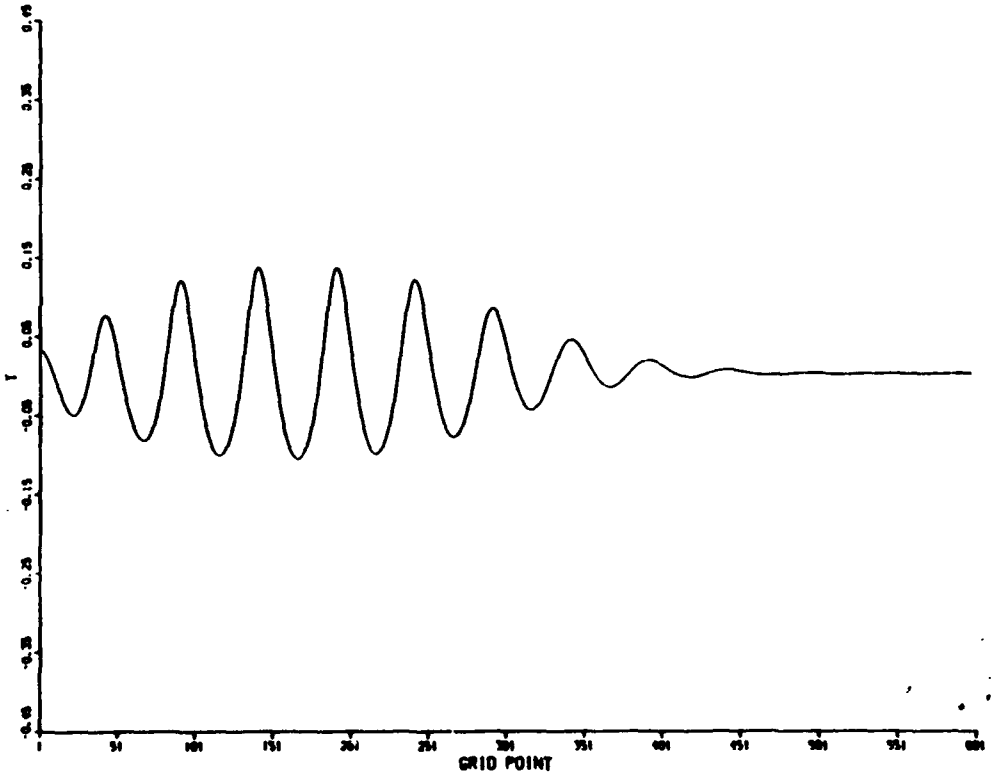

Fig. 1(d) — Details of the scene near the left wall at t = 56

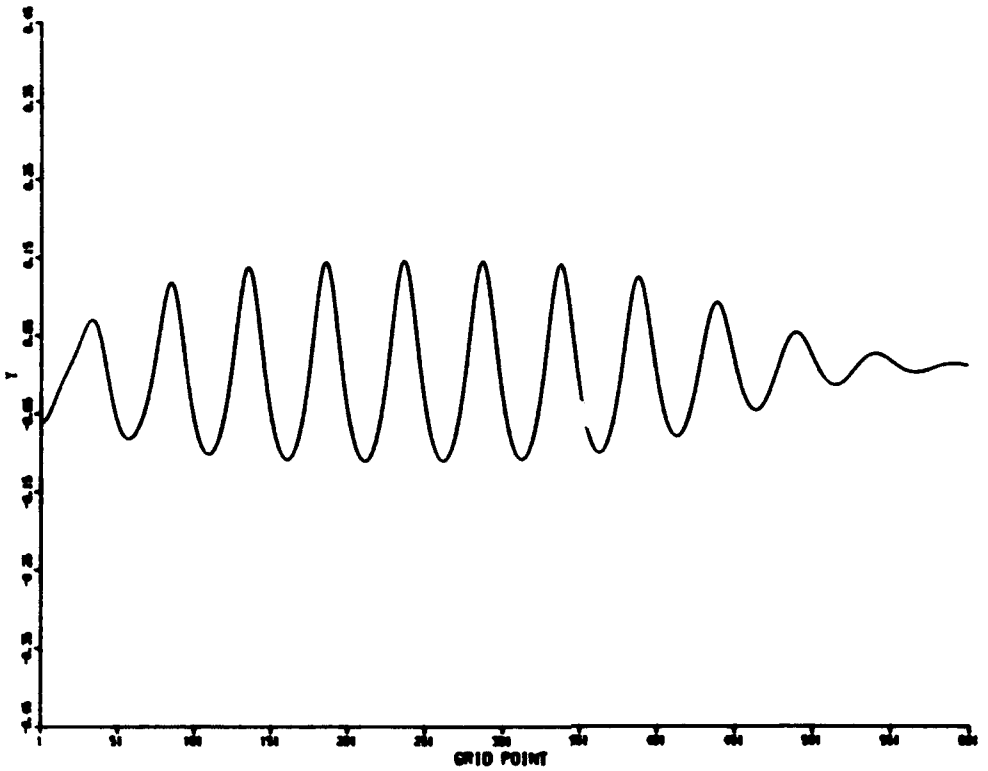

Fig. 1(e) — Details of the scene near the left wall at t = 84

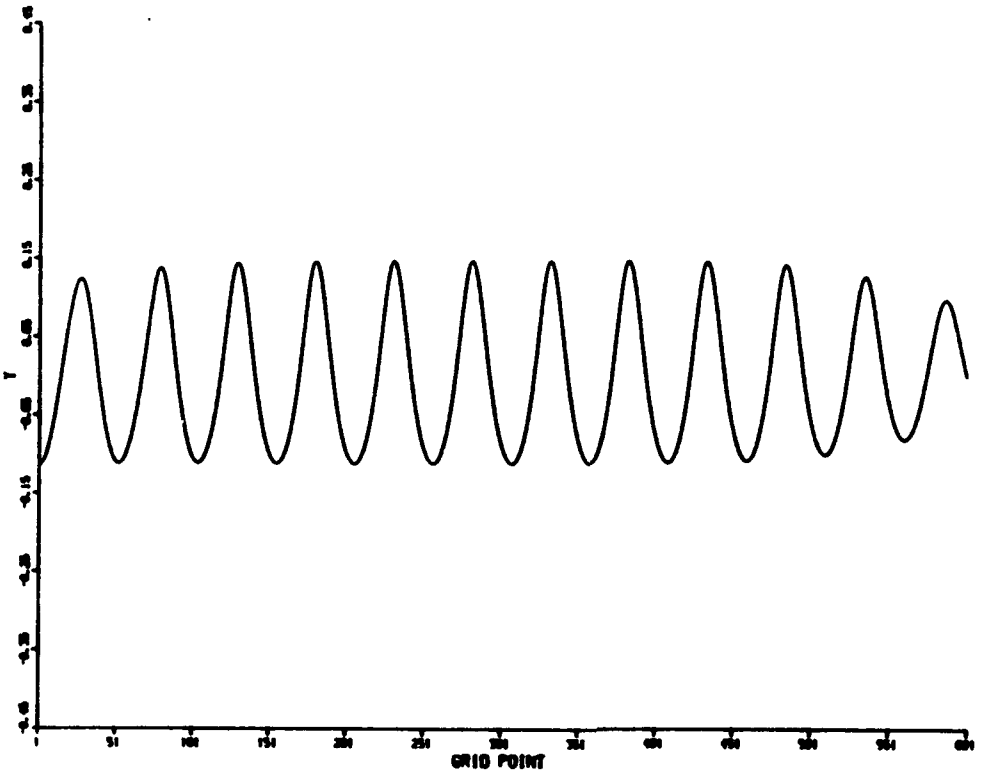

Fig. 1(f) — Details of the scene near the left wall at t = 112

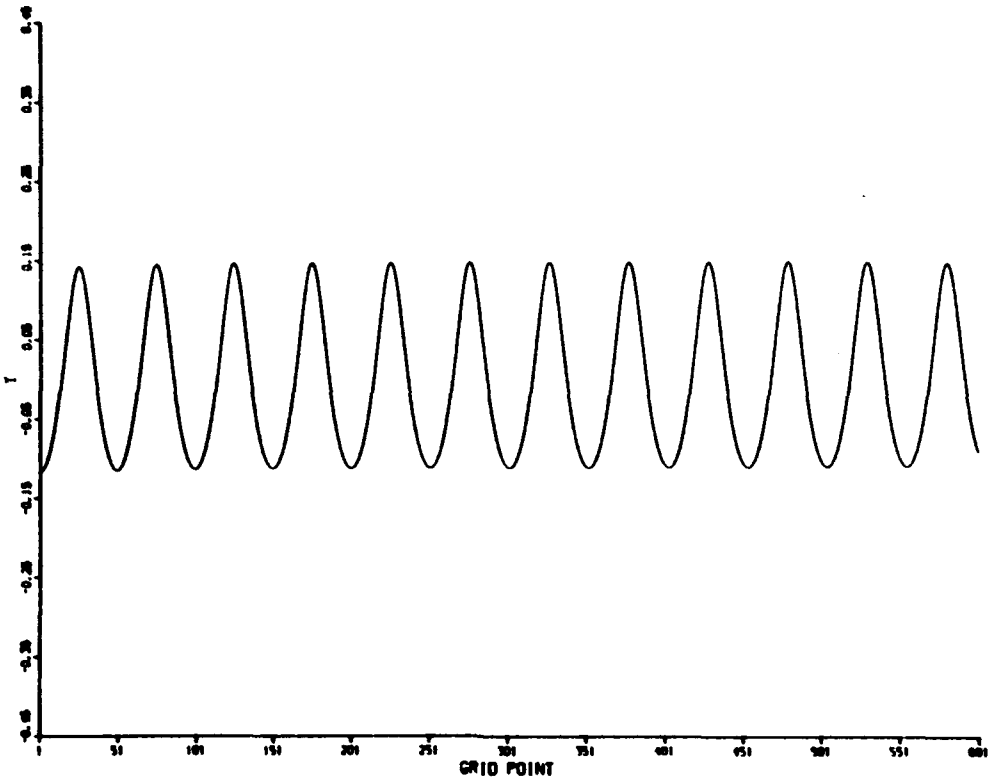

Fig. 1(g) — Details of the scene near the left wall at t = 140

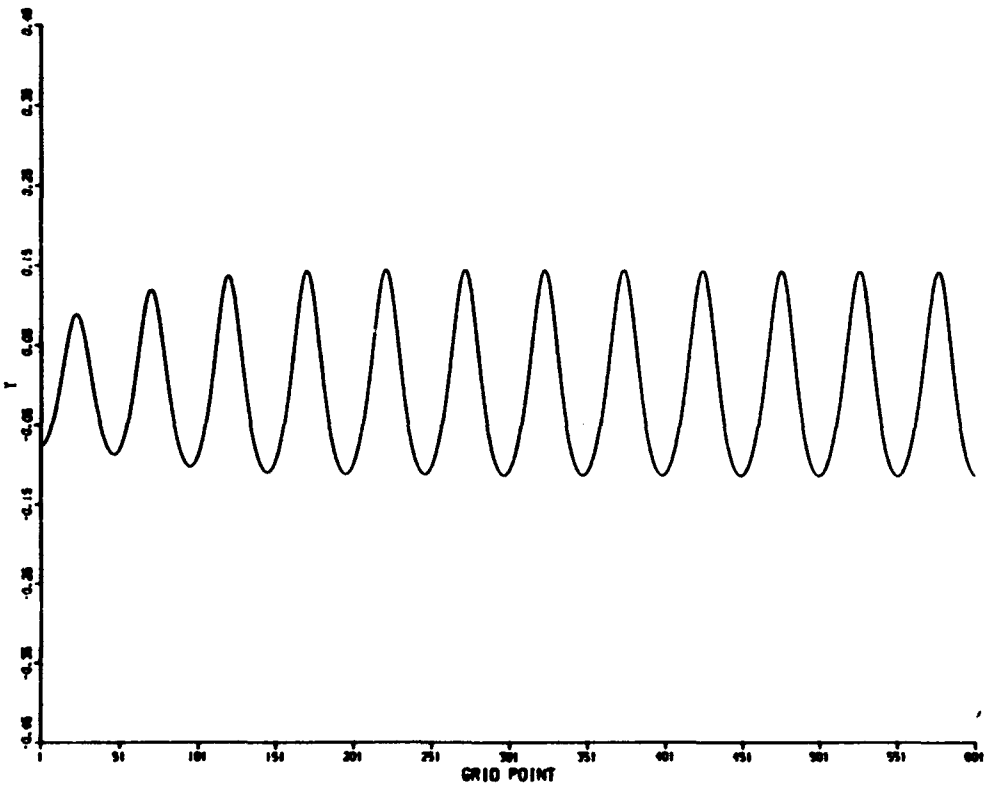

Fig. 1(h) — Details of the scene near the left wall at t = 168

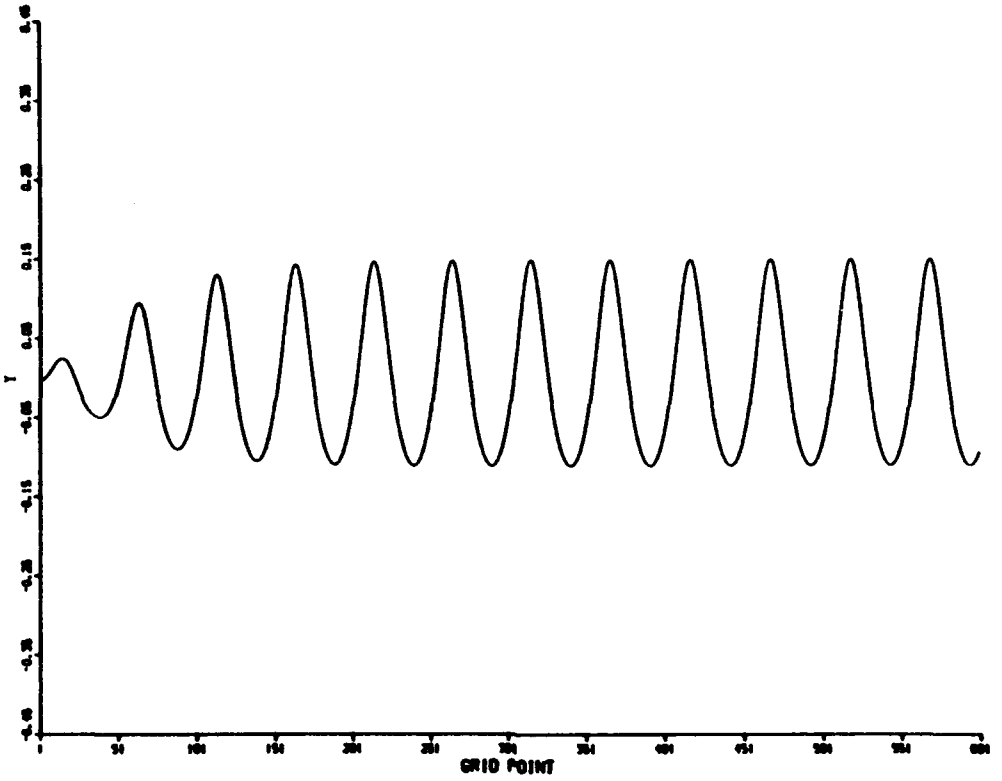

Fig. 1(i) — Details of the scene near the left wall at t = 196

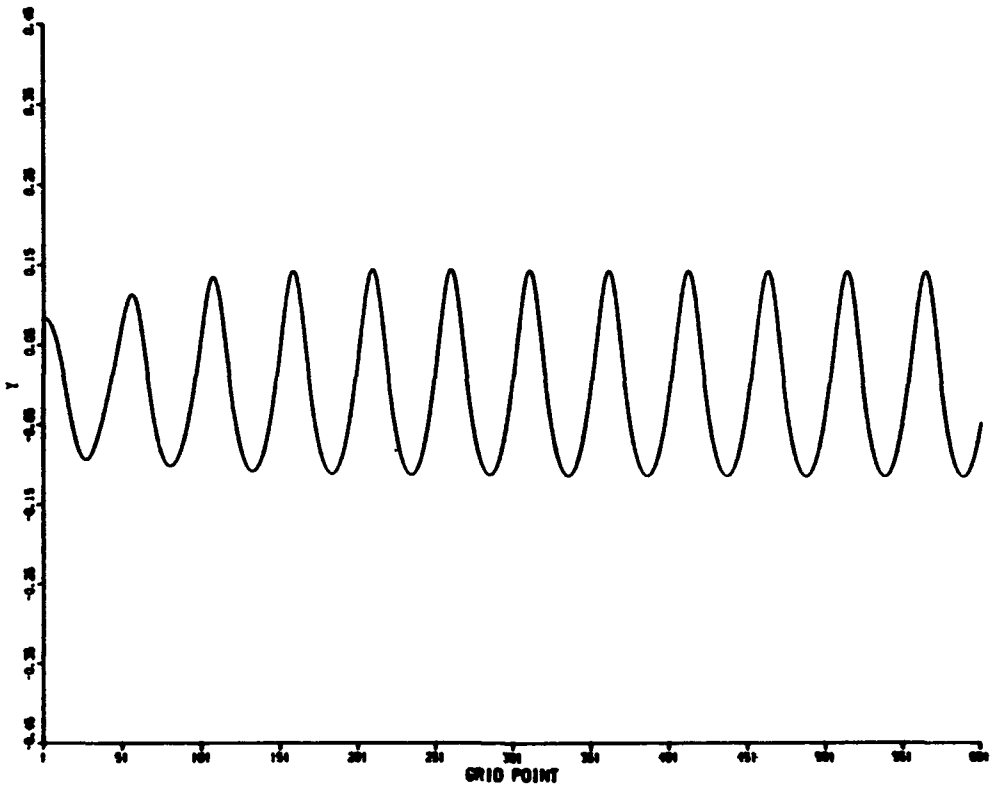

Fig. 1(j) — Details of the scene near the left wall at t = 224

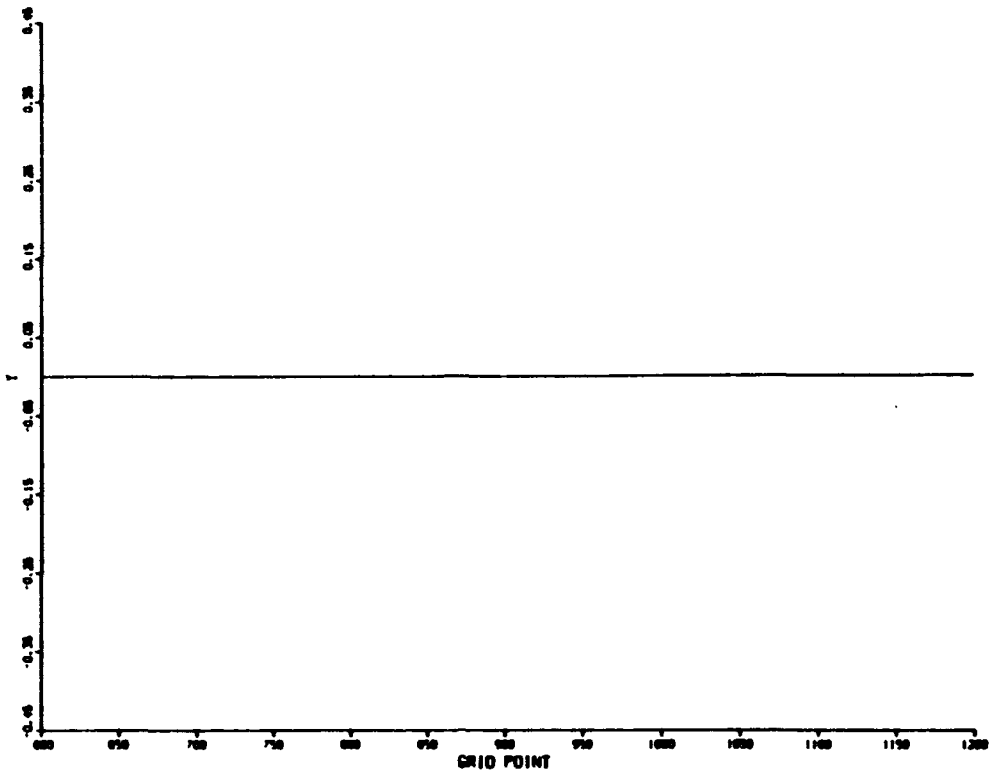

Fig. 1(k) — Details of the scene over the shoaling portion of the channel, between x = 75 (grid point 600) and x = 150 (grid point 1200). The shoaling starts at x = 80 (grid point 640) and continues to x = 160 (grid point 1280, outside these figures) at t = 28

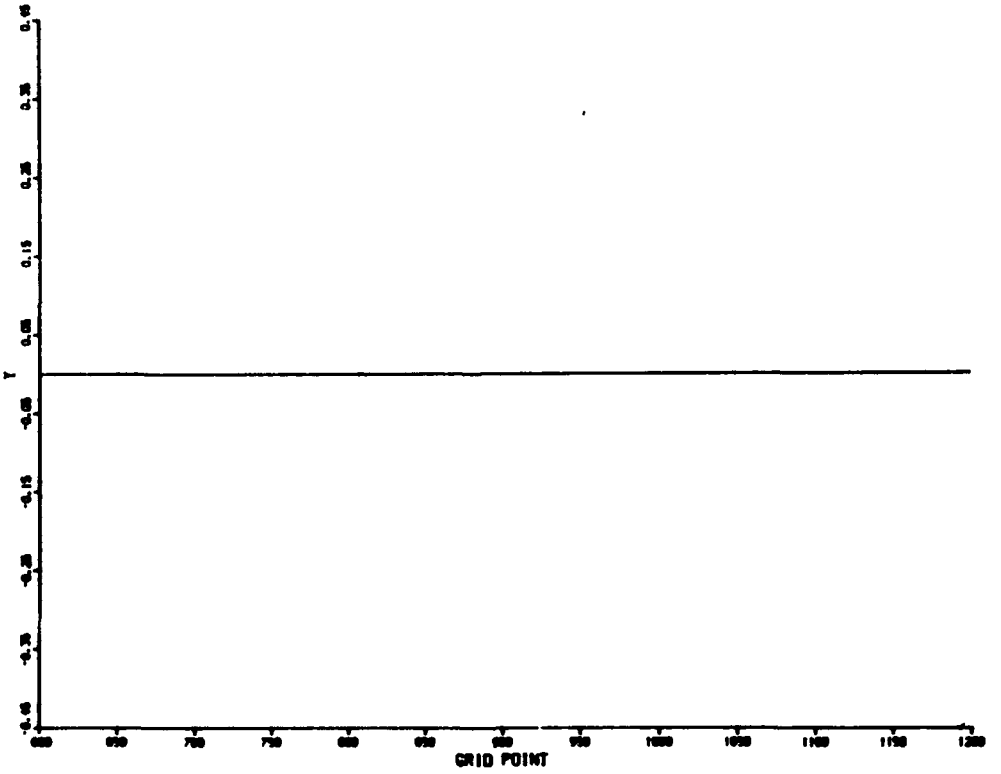

Fig. 1(l) — Details of the scene over the shoaling portion of the channel, between x = 75 (grid point 600) and x = 150 (grid point 1200). The shoaling starts at x = 80 (grid point 640) and continues to x = 160 (grid point 1280, outside these figures) at t = 56

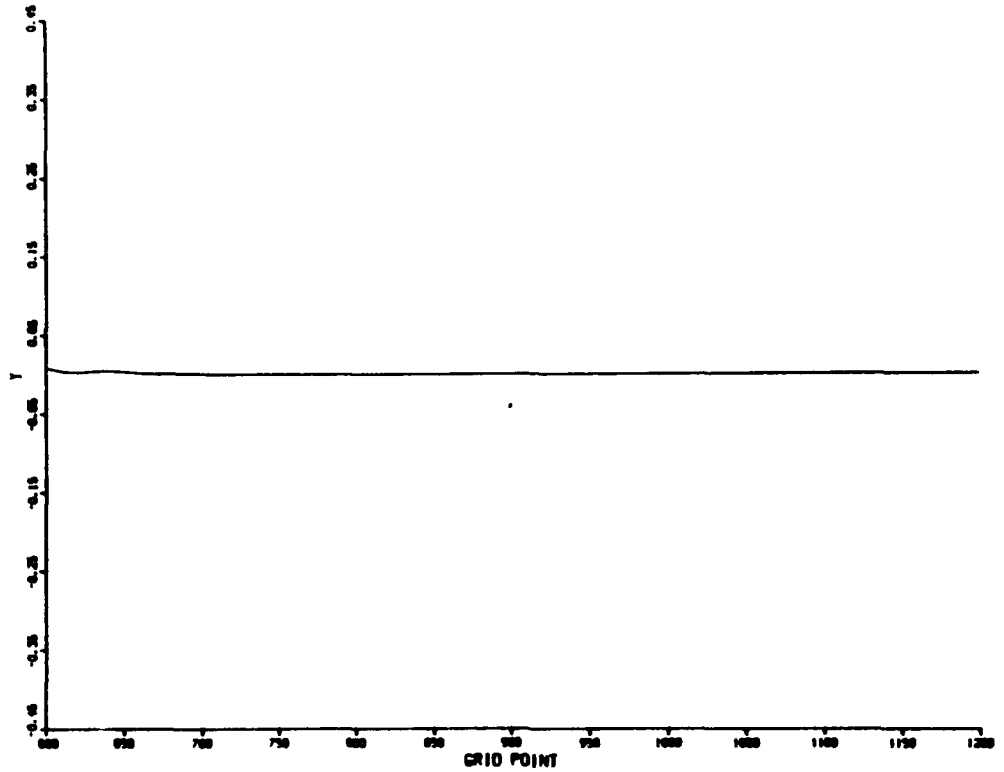

Fig. 1(m) — Details of the scene over the shoaling portion of the channel, between x = 75 (grid point 600) and x = 150 (grid point 1200). The shoaling starts at x = 80 (grid point 640) and continues to x = 160 (grid point 1280, outside these figures) at t = 84

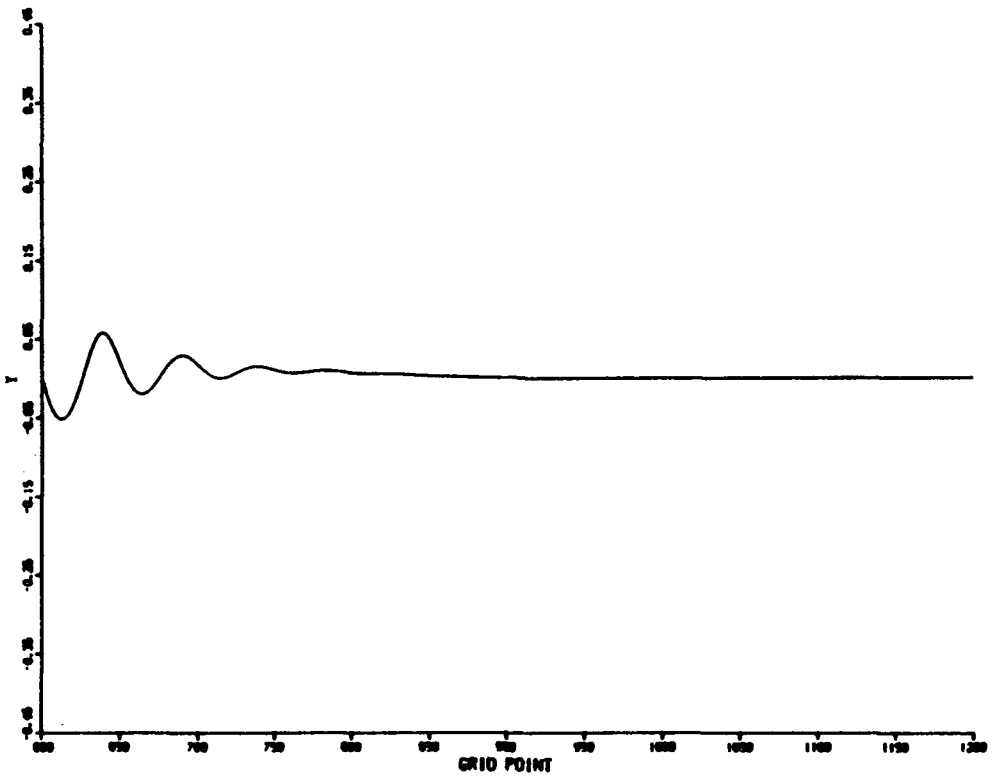

Fig. 1(n) — Details of the scene over the shoaling portion of the channel, between x = 75 (grid point 600) and x = 150 (grid point 1200). The shoaling starts at x = 80 (grid point 640) and continues to x = 160 (grid point 1280, outside these figures) at t = 112

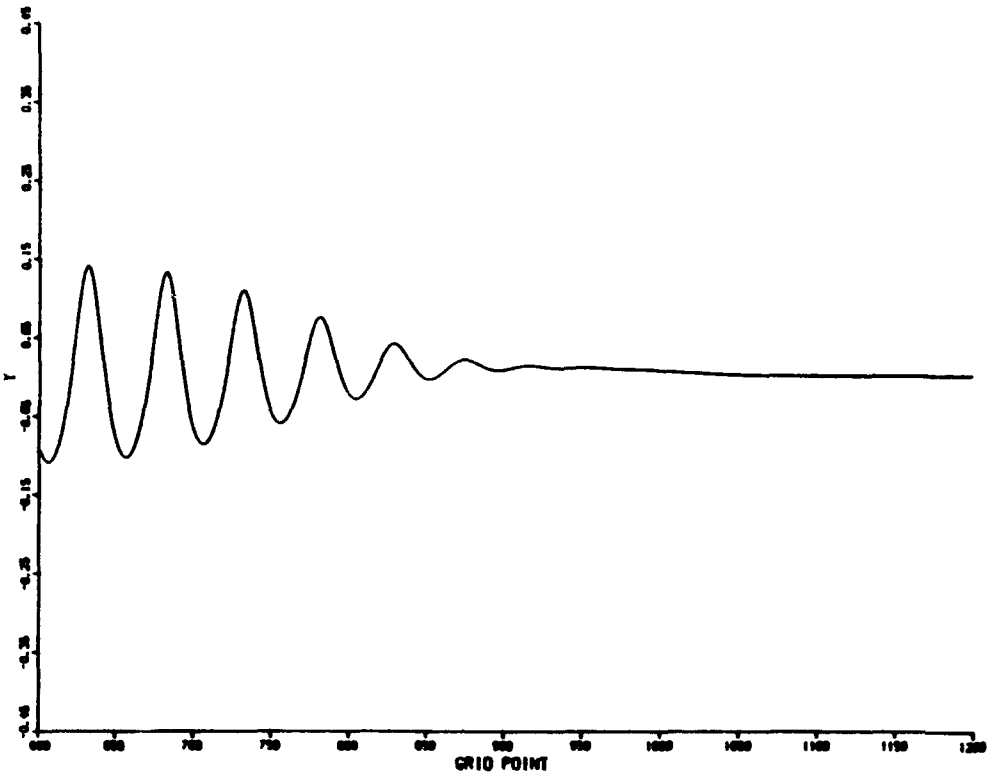

Fig. 1(o) — Details of the scene over the shoaling portion of the channel, between x = 75 (grid point 600) and x = 150 (grid point 1200). The shoaling starts at x = 80 (grid point 640) and continues to x = 160 (grid point 1280, outside these figures) at t = 140

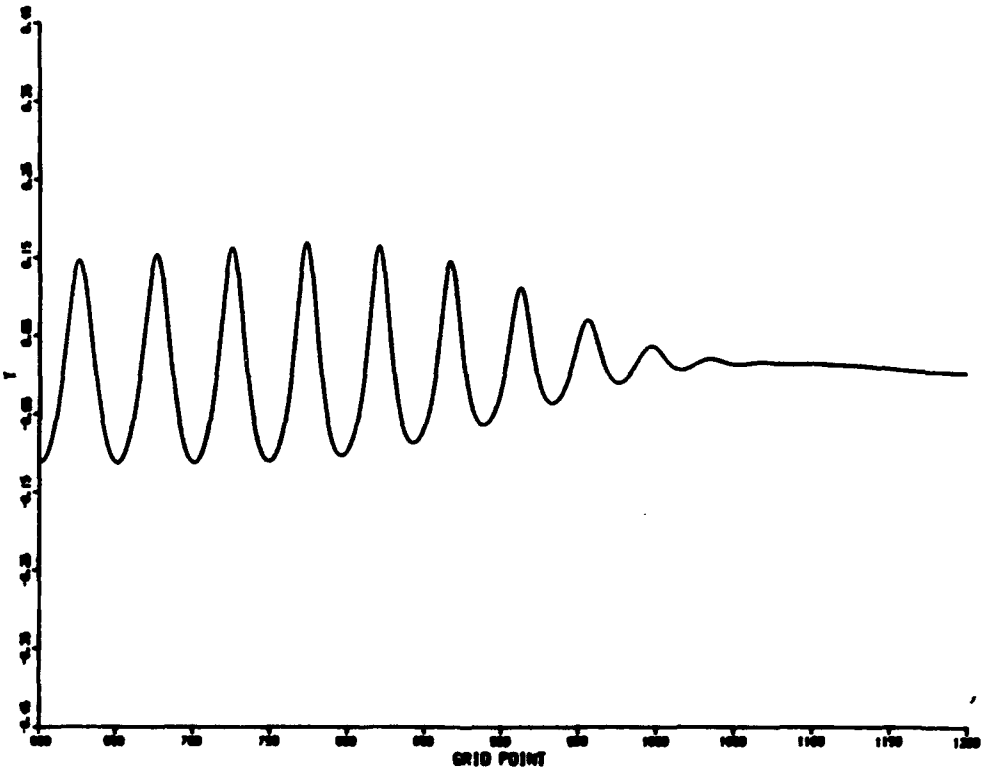

Fig. 1(p) — Details of the scene over the shoaling portion of the channel, between x = 75 (grid point 600) and x = 150 (grid point 1200). The shoaling starts at x = 80 (grid point 640) and continues to x = 160 (grid point 1280, outside these figures) at t = 168

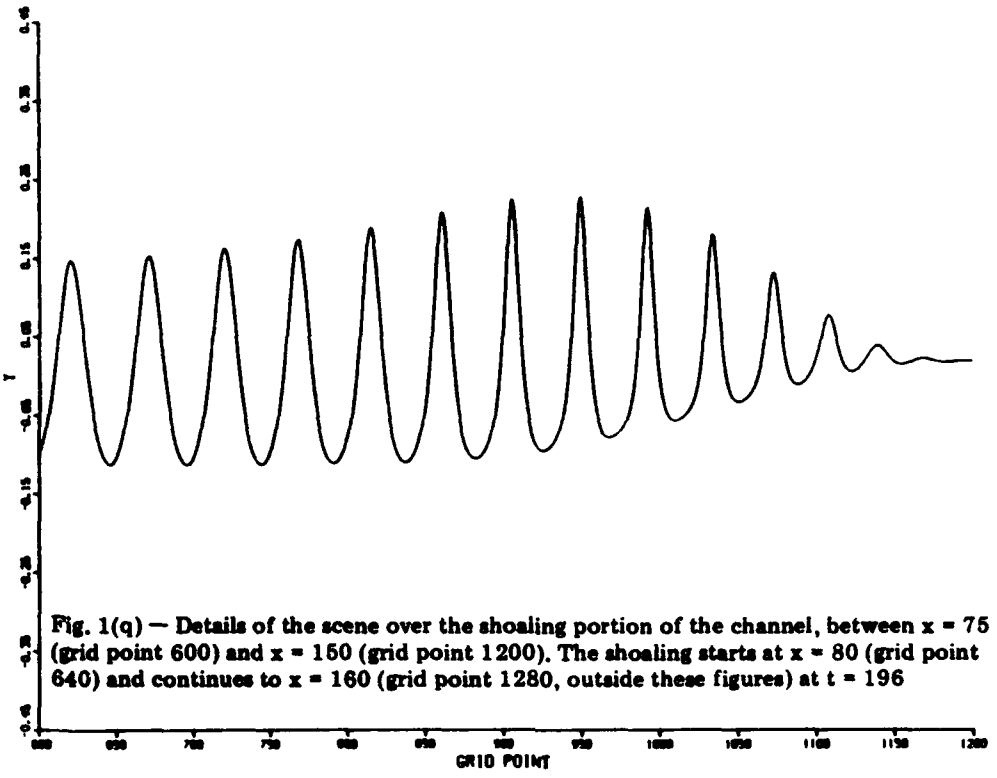

Fig. 1(q) — Details of the scene over the shoaling portion of the channel, between x = 75 (grid point 600) and x = 150 (grid point 1200). The shoaling starts at x = 80 (grid point 640) and continues to x = 160 (grid point 1280, outside these figures) at t = 196

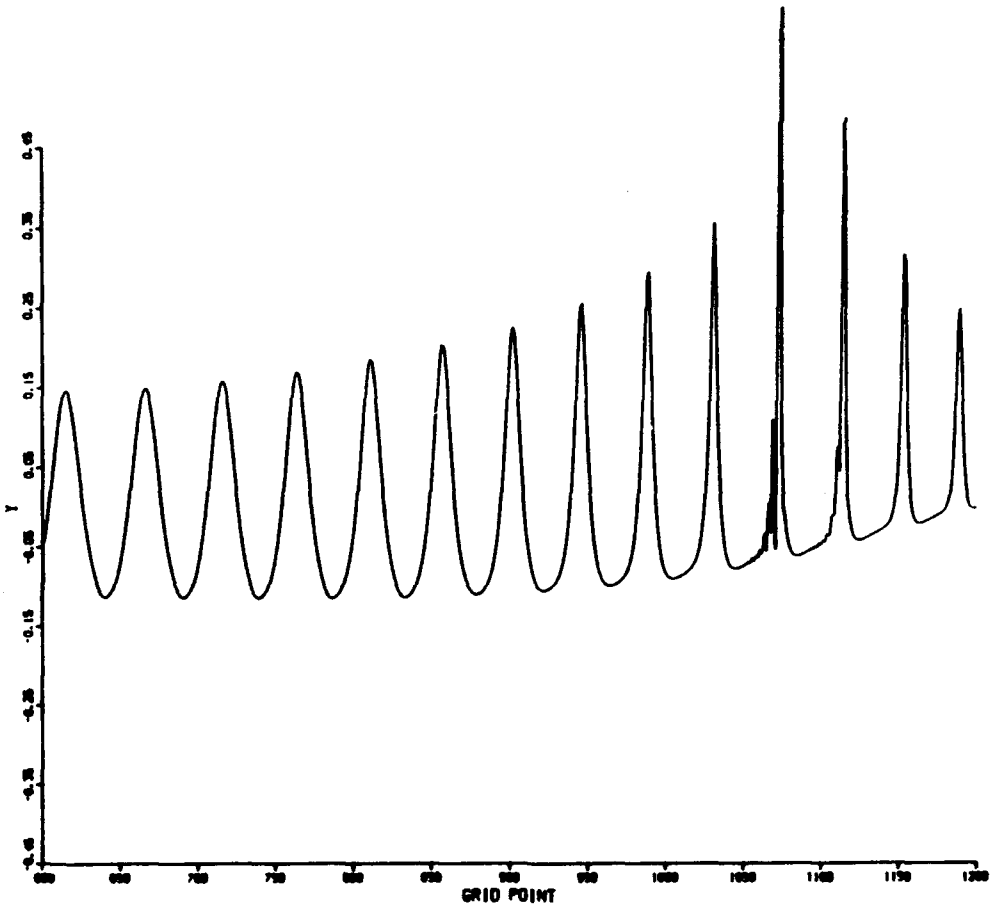

Fig. 1(r) — Details of the scene over the shoaling portion of the channel, between x = 75 (grid point 600) and x = 150 (grid point 1200). The shoaling starts at x = 80 (grid point 640) and continues to x = 160 (grid point 1280, outside these figures) at t = 224

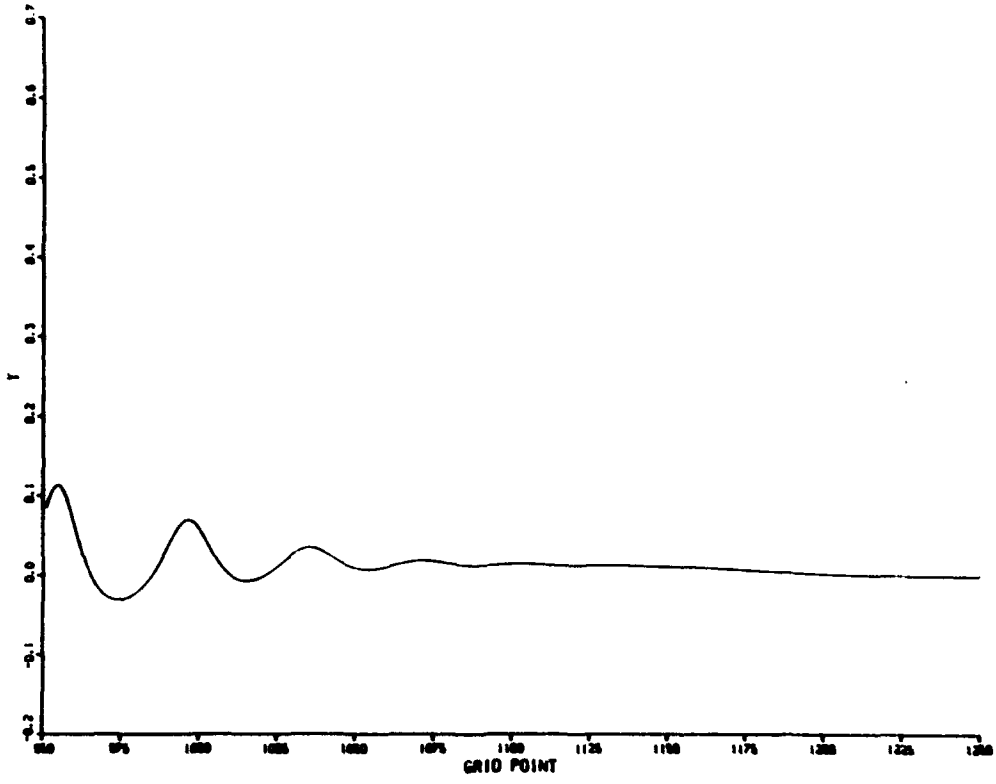

Fig. 1(s) — Further details of the scene between x = 118.75 (grid point 950) and x = 156.25 (grid point 1250) at t = 175

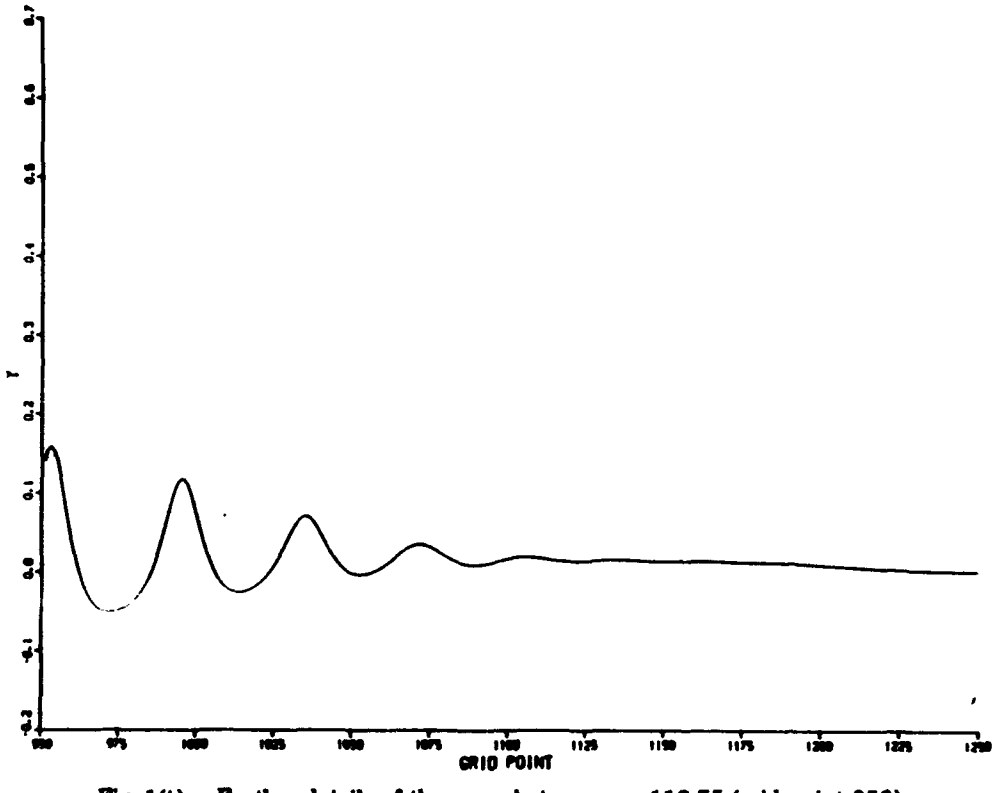

Fig. 1(t) — Further details of the scene between x = 118.75 (grid point 950) and x = 156.25 (grid point 1250) at t = 182

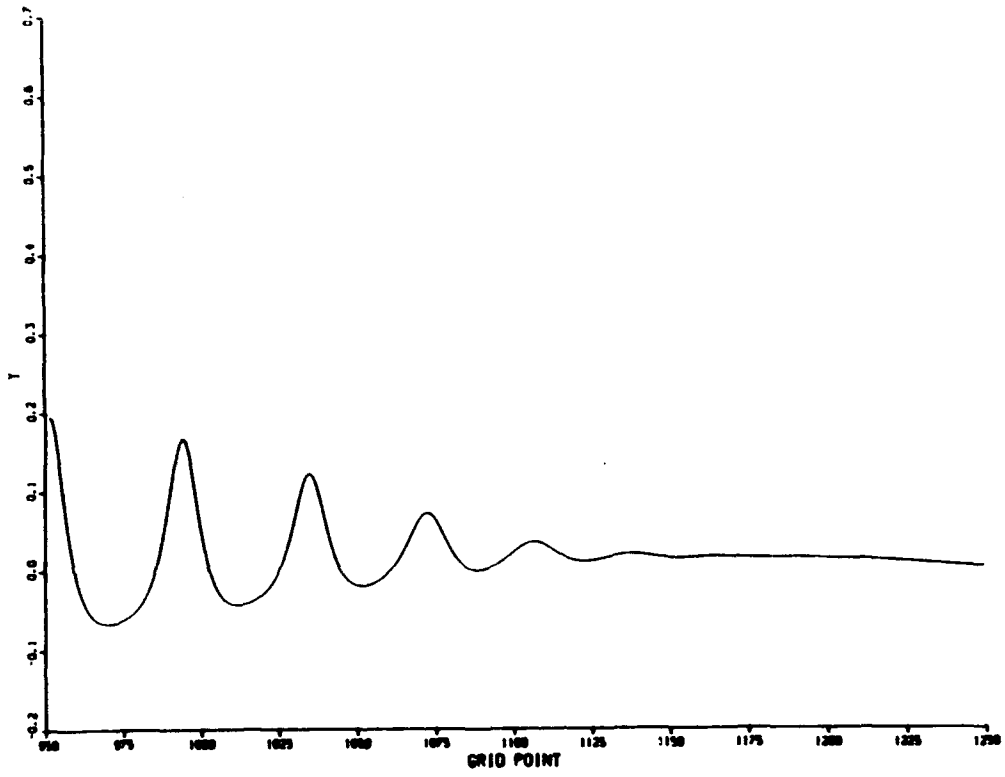

Fig. 1(u) — Further details of the scene between x = 118.75 (grid point 950) and x = 156.25 (grid point 1250) at t = 189

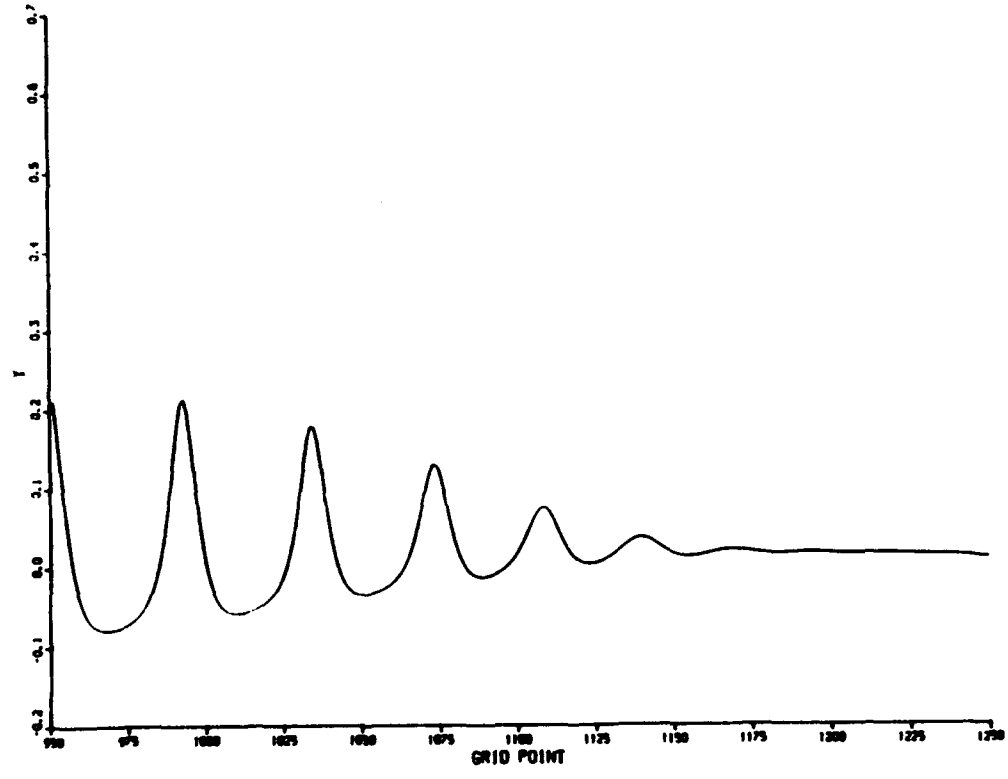

Fig. 1(v) — Further details of the scene between x = 118.75 (grid point 950) and x = 156.25 (grid point 1250) at t = 196

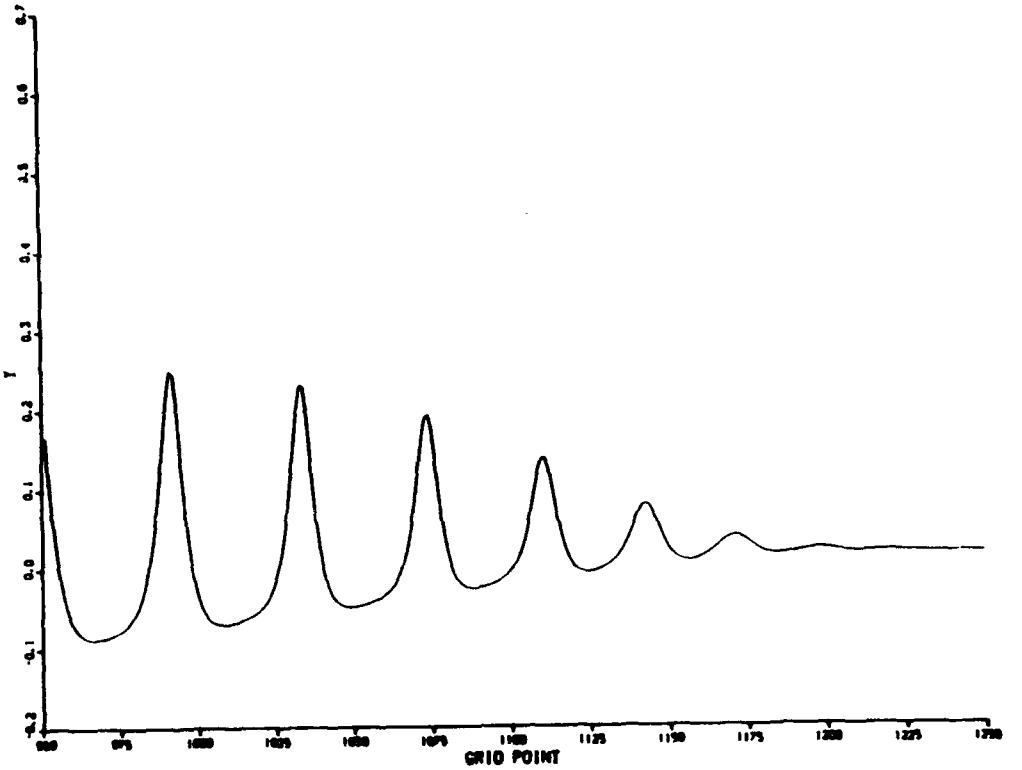

Fig. 1(w) — Further details of the scene between x = 118.75 (grid point 950) and x = 156.25 (grid point 1250) at t = 203

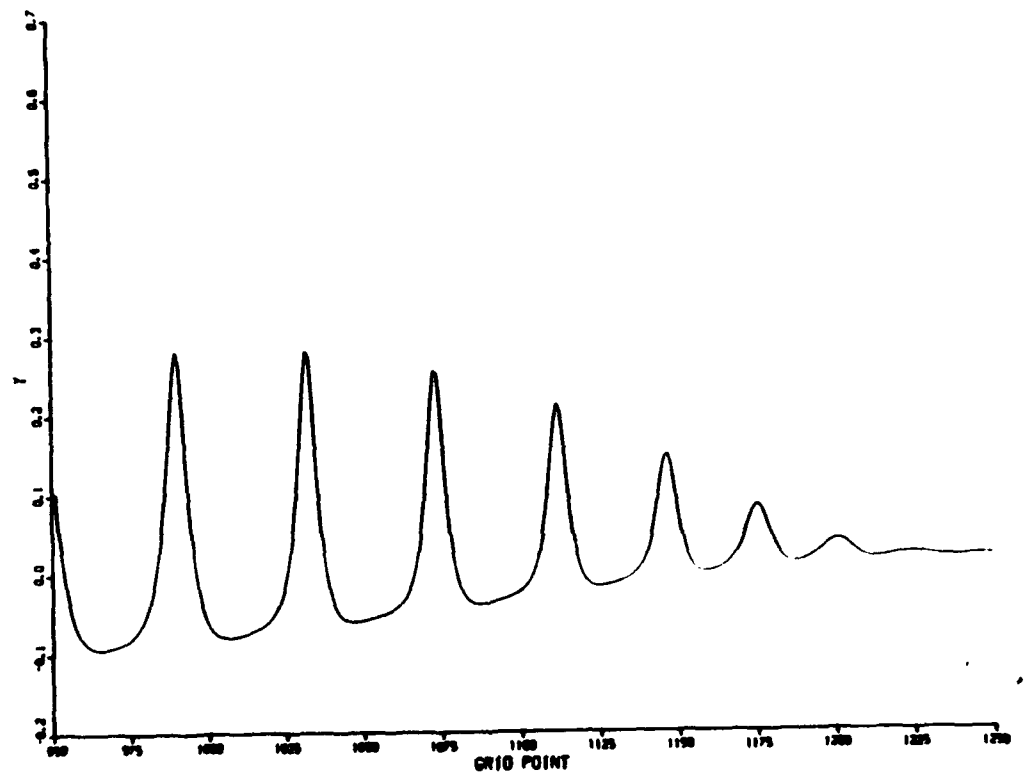

Fig. 1(x) — Further details of the scene between x = 118.75 (grid point 950) and x = 156.25 (grid point 1250) at t = 210

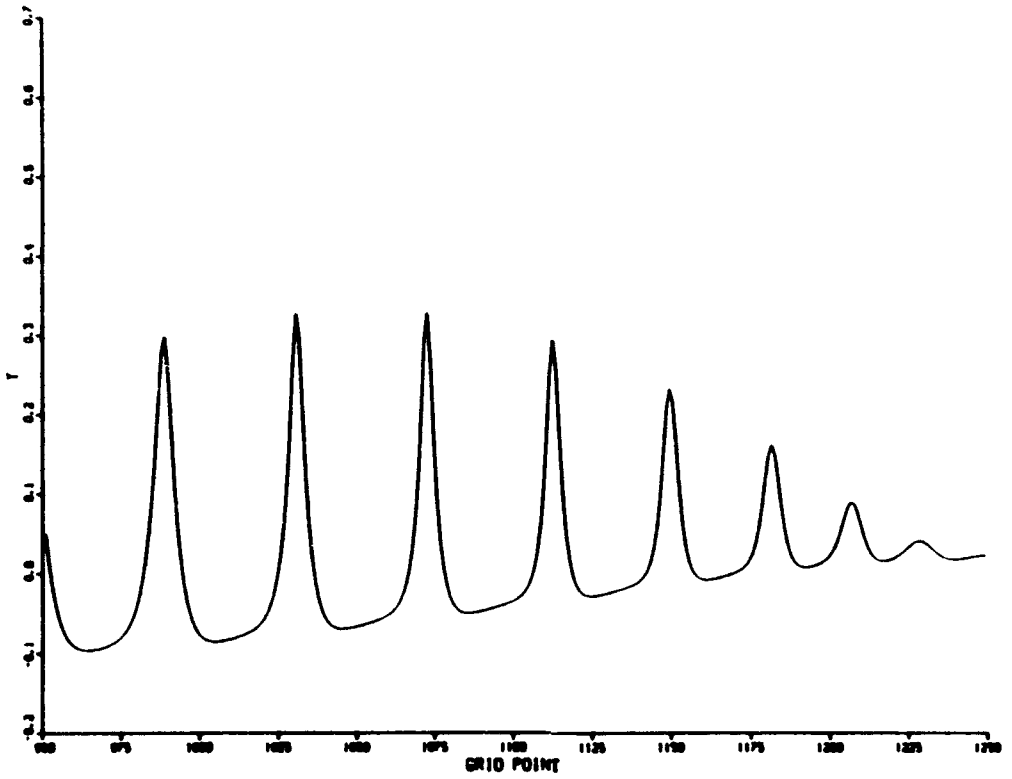

Fig. 1(y) — Further details of the scene between x = 118.75 (grid point 950) and x = 156.25 (grid point 1250) at t = 217

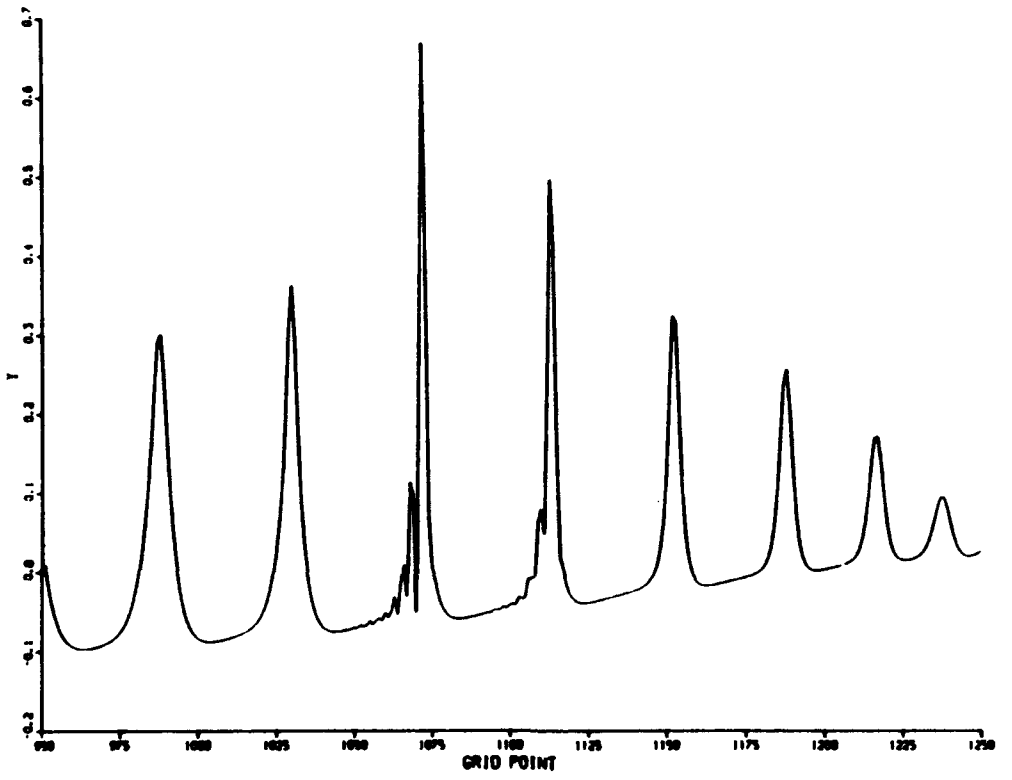

Fig. 1(z) — Further details of the scene between x = 118.75 (grid point 950) and x = 156.25 (grid point 1250) at t = 224

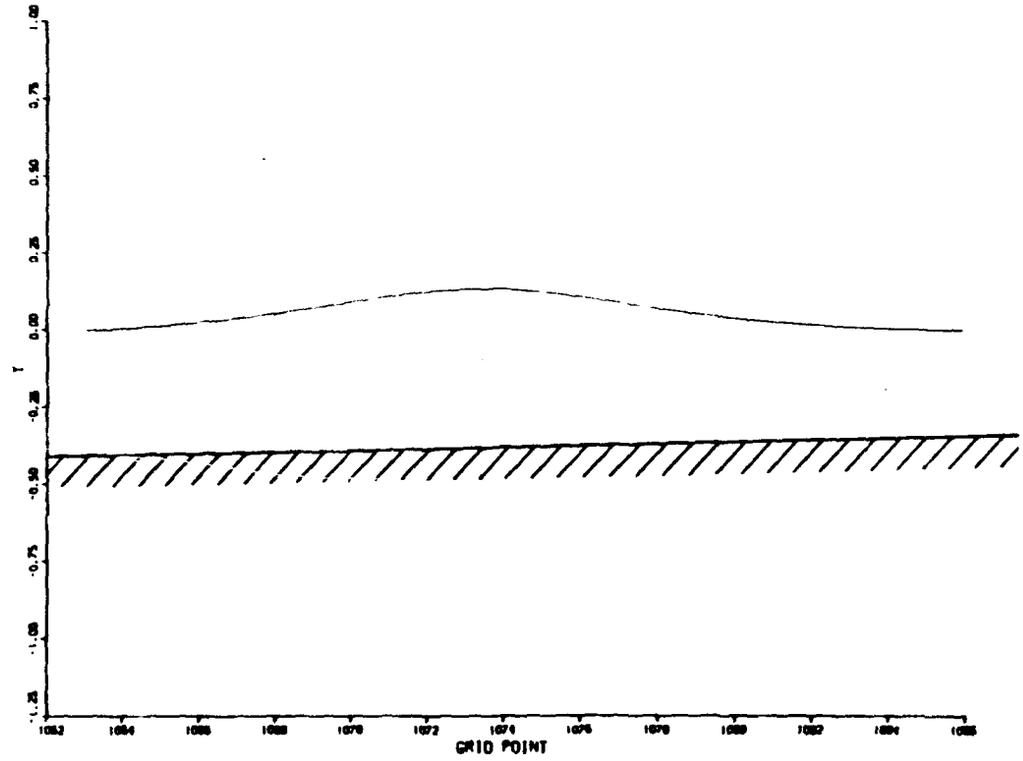

Fig. 1(aa) — The scene between x = 132.375 (grid point 1063) and x = 135.75 (grid point 1086). The horizontal and vertical scales are the same: at t = 196.

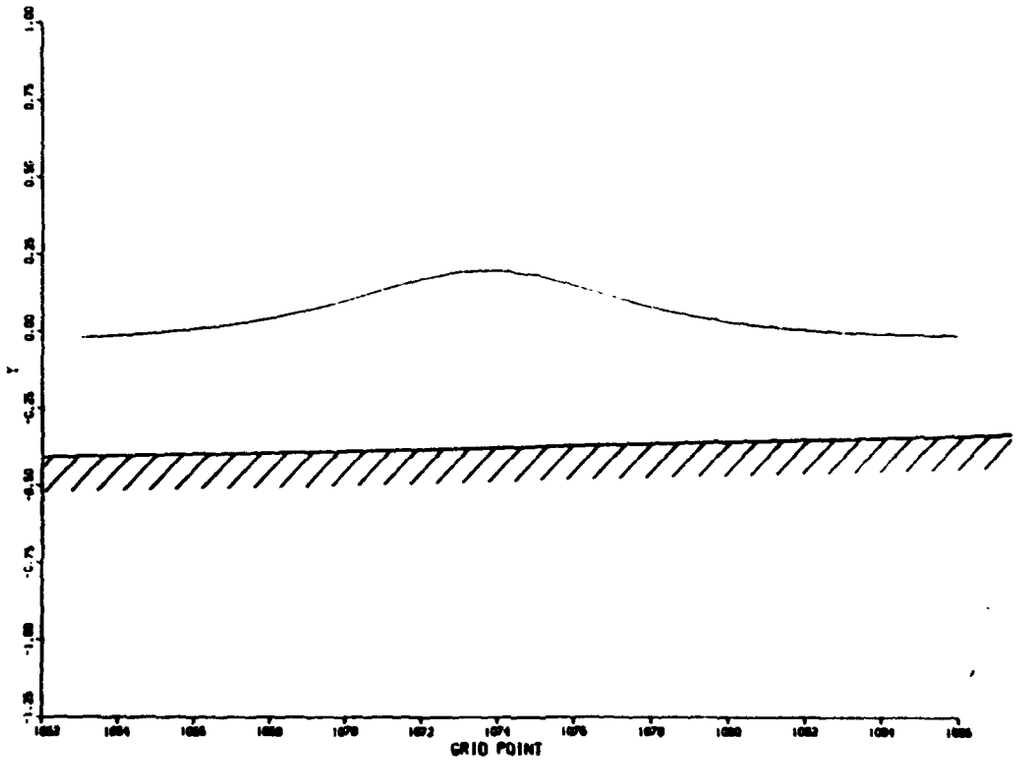

Fig. 1(bb) — The scene between x = 132.375 (grid point 1063) and x = 135.75 (grid point 1086). The horizontal and vertical scales are the same: at t = 203.

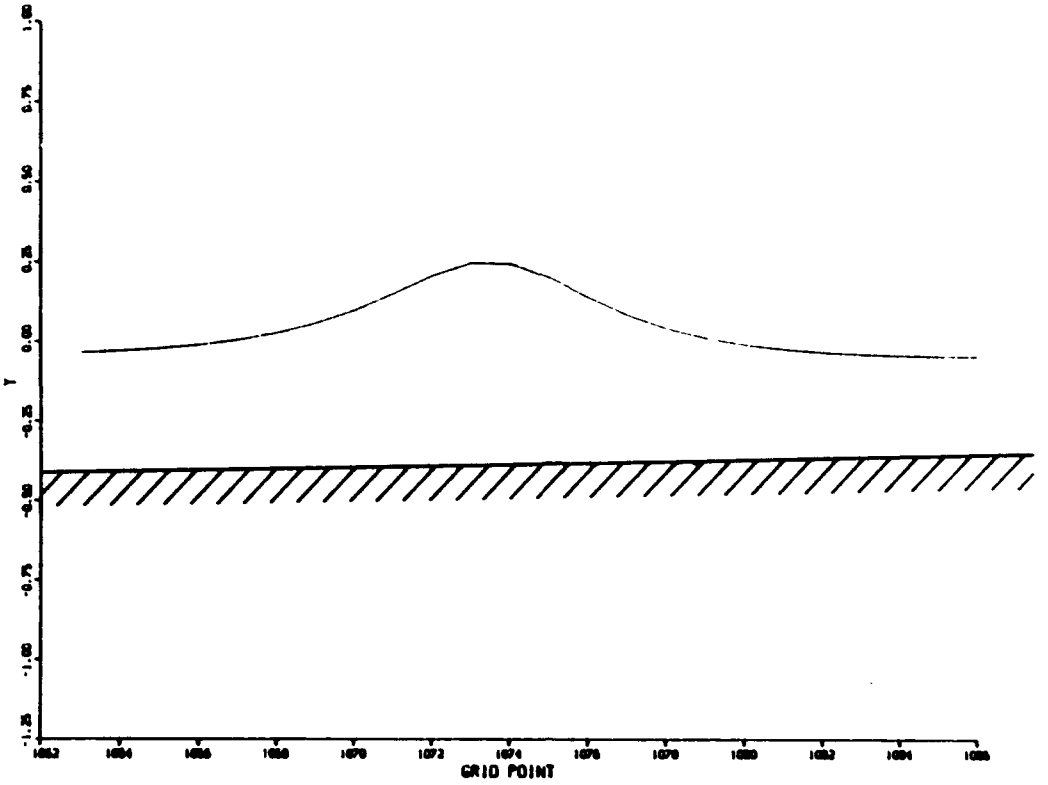

Fig. 1(cc) — The scene between x = 132.375 (grid point 1063) and x = 135.75 (grid point 1086). The horizontal and vertical scales are the same: at t = 210.

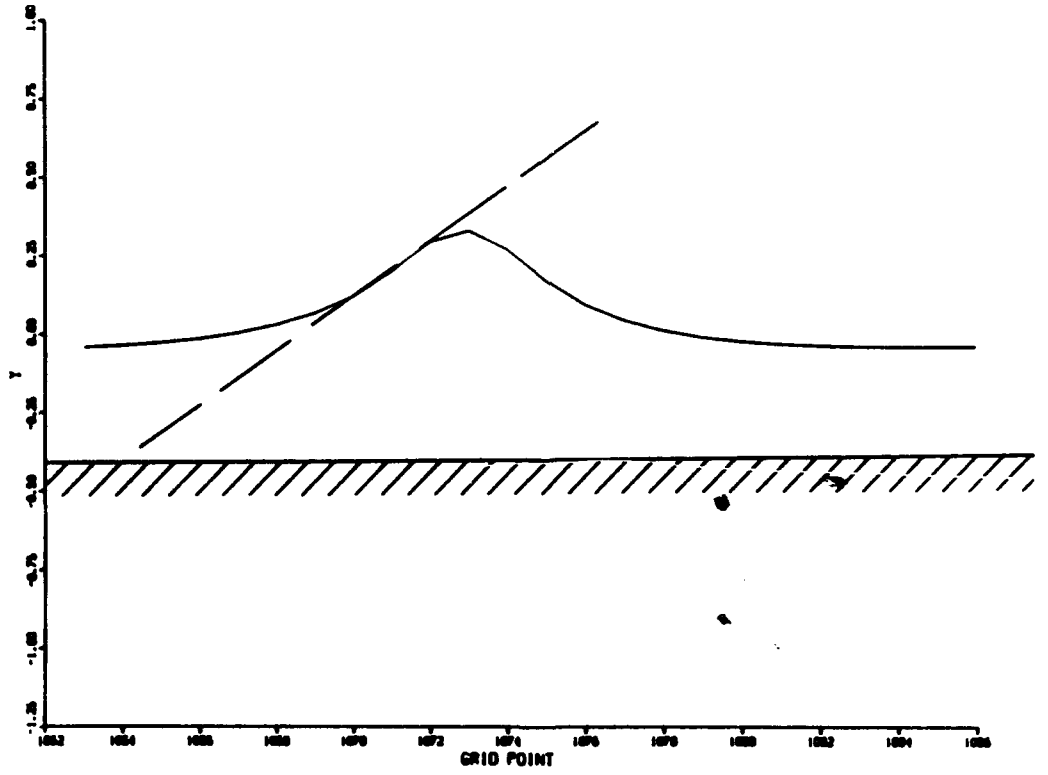

Fig. 1(dd) — The scene between x = 132.375 (grid point 1063) and x = 135.75 (grid point 1086). The horizontal and vertical scales are the same: at t = 217. The wave's maximum slope and amplitude exceed those of a breaking progressive wave.

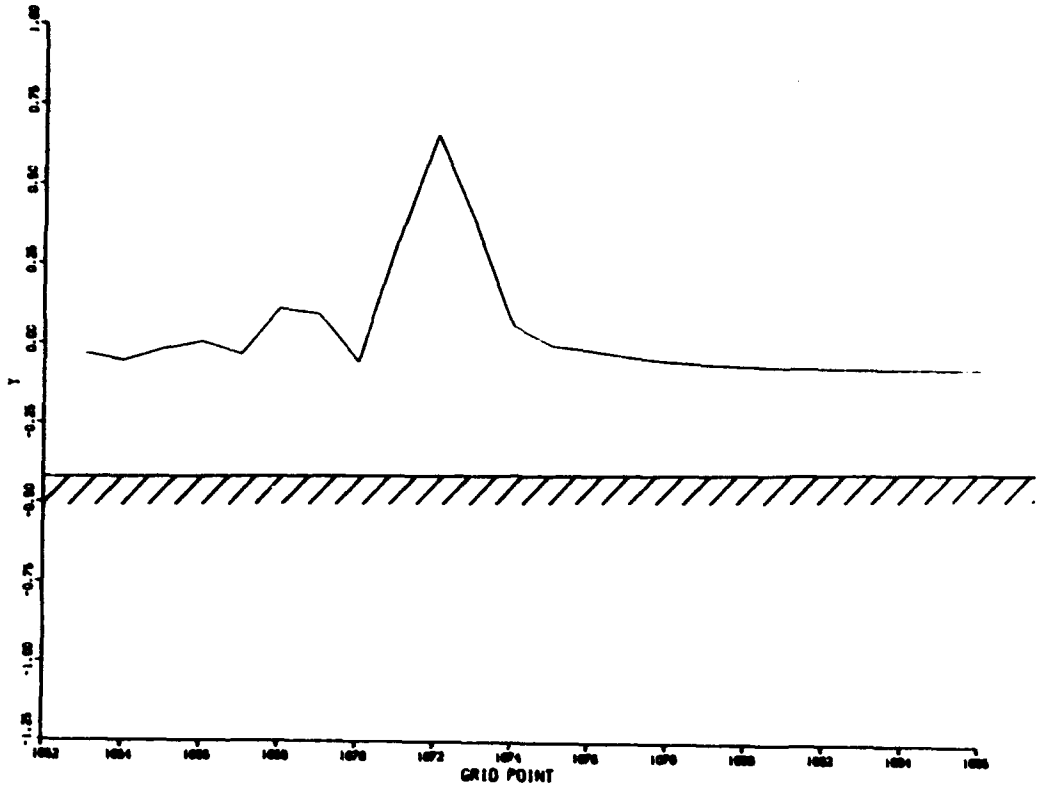

Fig. 1(ee) — The scene between x = 132.375 (grid point 1063) and x = 135.75 (grid point 1086). The horizontal and vertical scales are the same: at t = 224. The calculation at this time is not very meaningful.

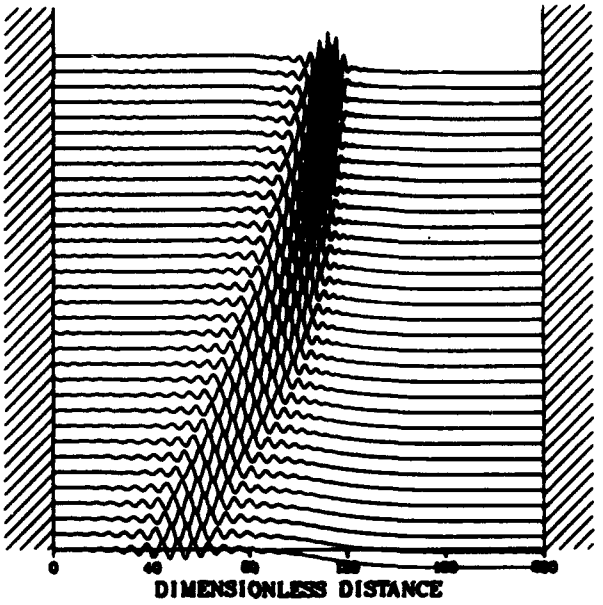

Fig. 2(a) — Blocking of a wave packet by an adverse nonuniform current; the curves show the surface elevation away from a mean level at successive times, starting at the bottom. Distance is measured in units of mean depth at the left side, h_0. The vertical distance between profiles is set so that a disturbance that travels at a speed $\sqrt{gh_0}$ would show up along a $\pm 53.1^\circ$ angle in the figure. The calculations were run with the unified waves model, a variable breadth (more constricted toward the right) and a steady flow from right to left that is faster at the right than at the left. The geometry and initial conditions are shown in Fig. 3.

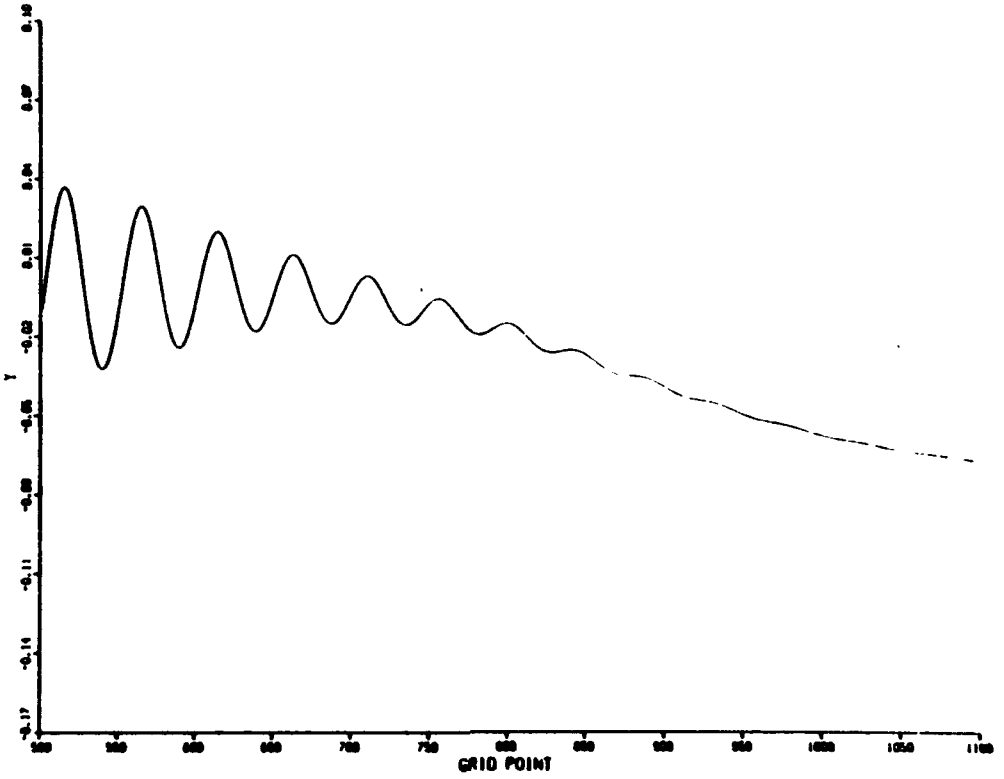

Fig. 2(b) — Details of the scene between x = 62.5 (grid point 500) and x = 137.5 (grid point 1100) at t = 117.19

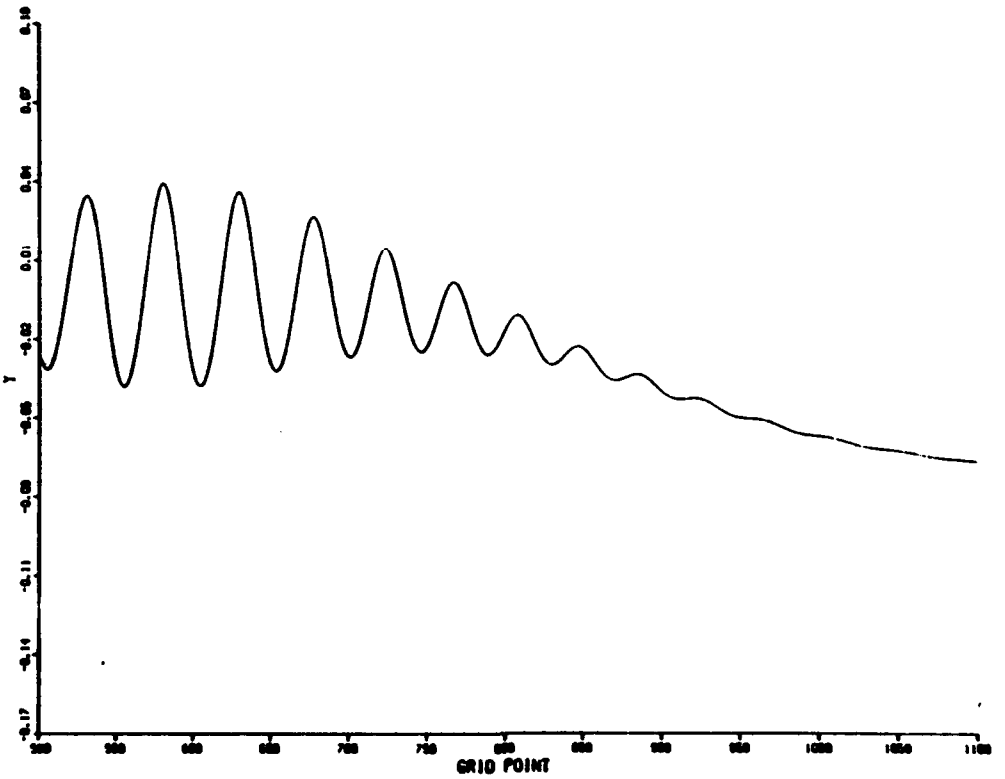

Fig. 2(c) — Details of the scene between x = 62.5 (grid point 500) and x = 137.5 (grid point 1100) at t = 121.88

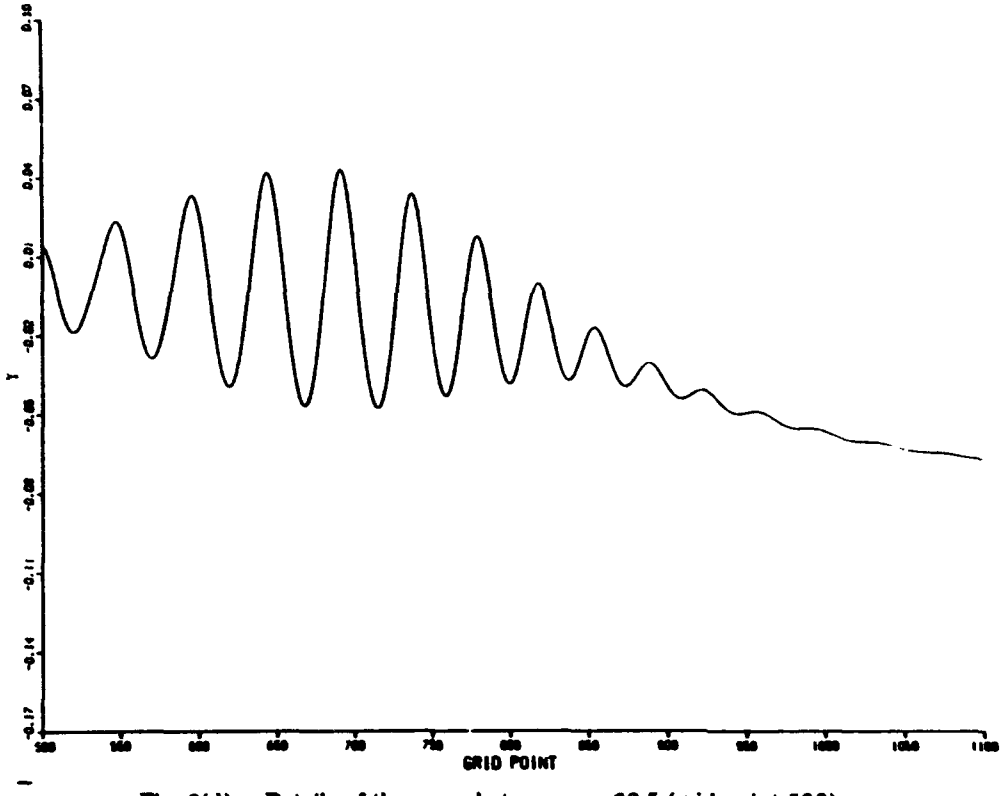

Fig. 2(d) — Details of the scene between x = 62.5 (grid point 500) and x = 137.5 (grid point 1100) at t = 126.56

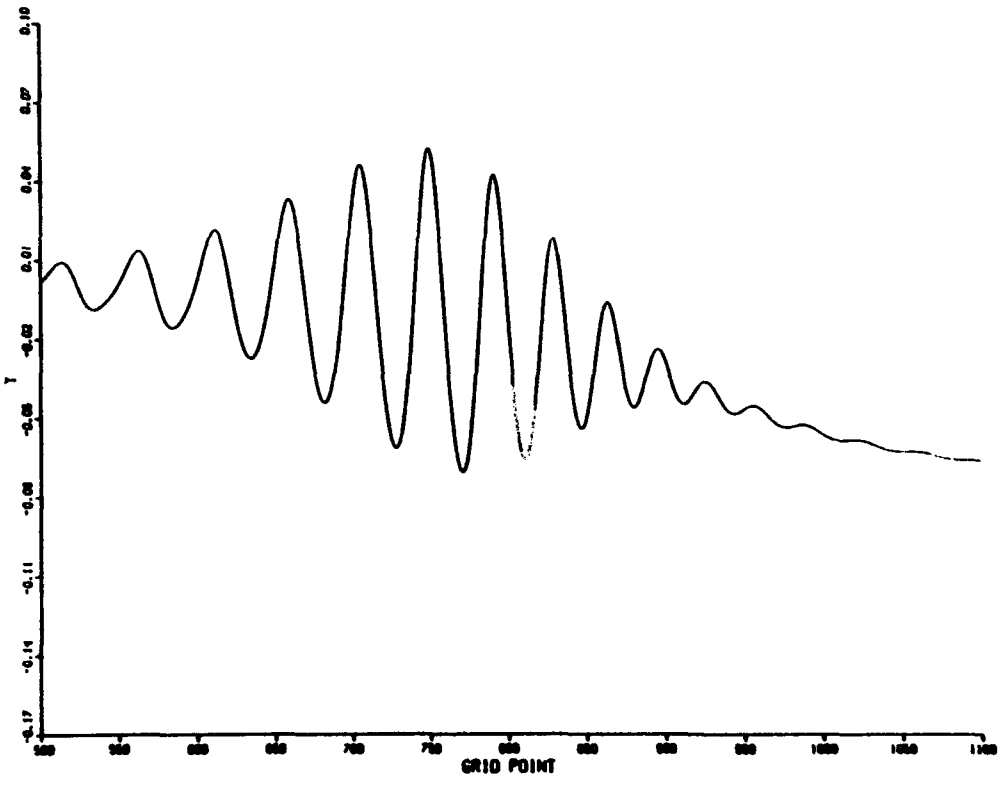

Fig. 2(e) — Details of the scene between x = 62.5 (grid point 500) and x = 137.5 (grid point 1100) at t = 131.25

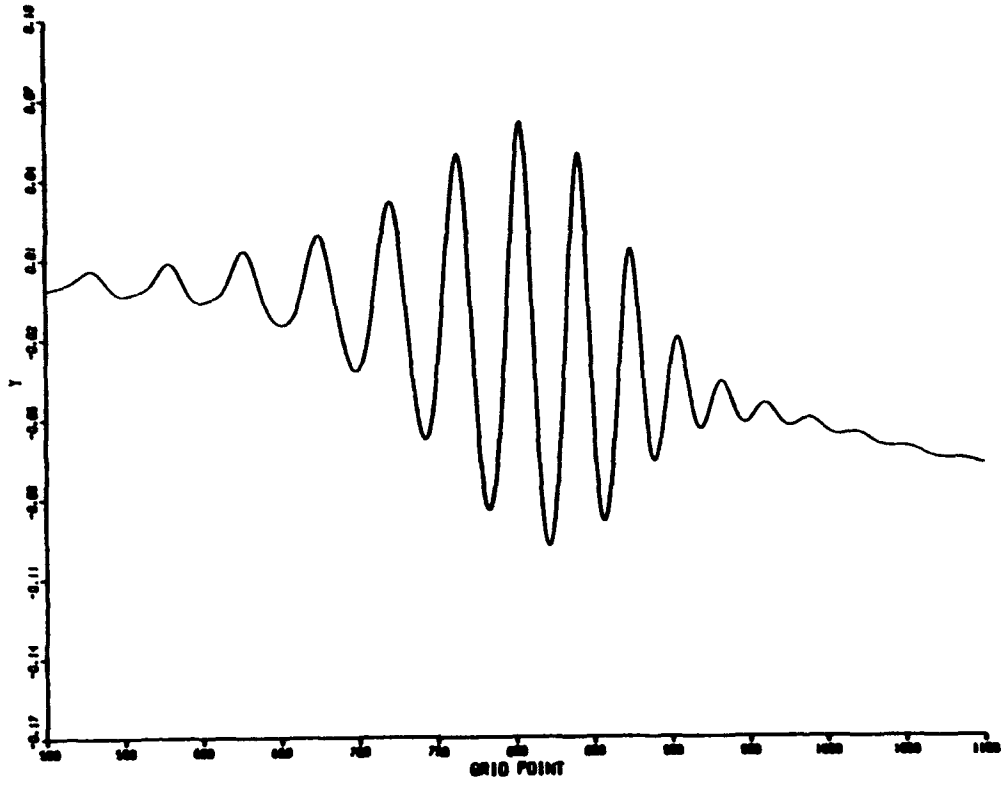

Fig. 2(f) — Details of the scene between x = 62.5 (grid point 500) and x = 137.5 (grid point 1100) at t = 135.94

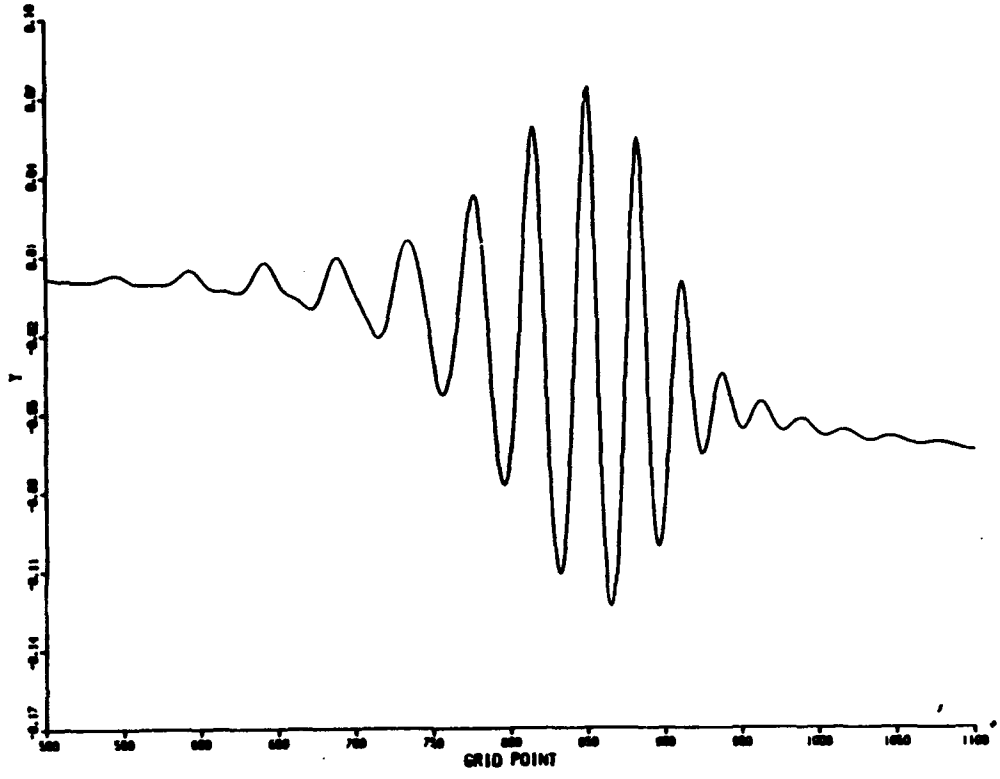

Fig. 2(g) — Details of the scene between x = 62.5 (grid point 500) and x = 137.5 (grid point 1100) at t = 140.63

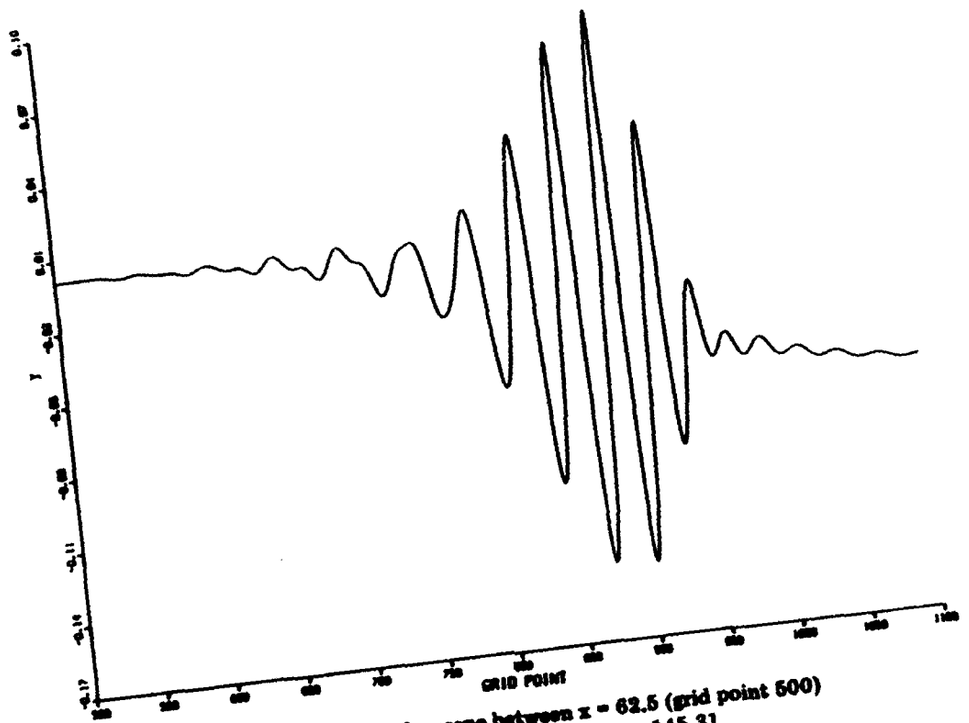

Fig. 2(h) — Details of the scene between x = 62.5 (grid point 500) and x = 137.5 (grid point 1100) at t = 145.31

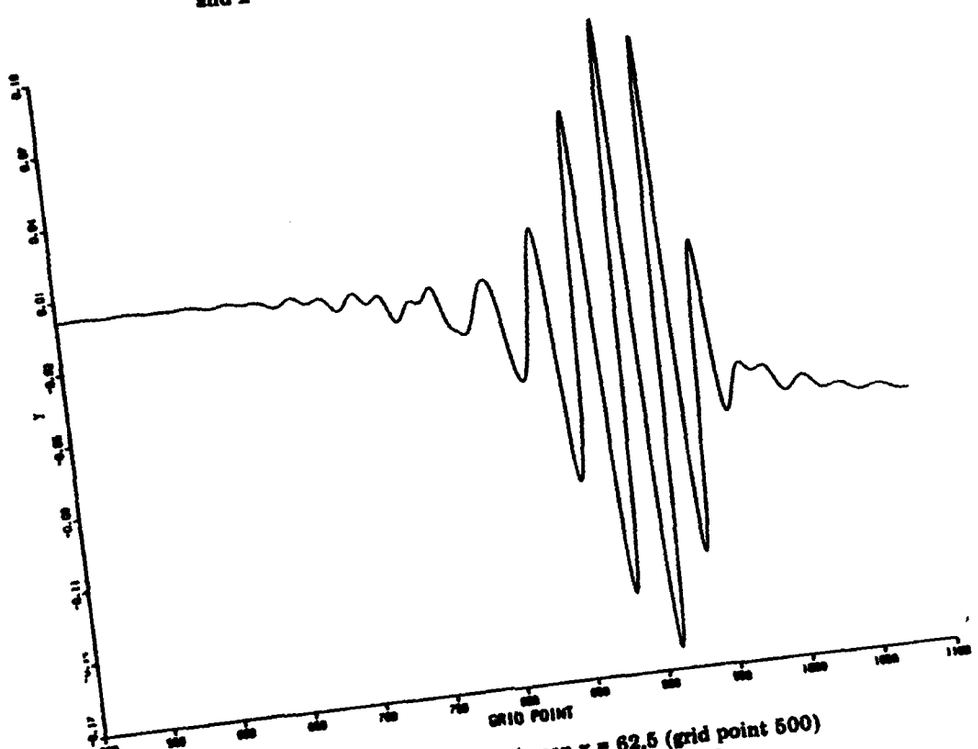

Fig. 2(i) — Details of the scene between x = 62.5 (grid point 500) and x = 137.5 (grid point 1100) at t = 150.00

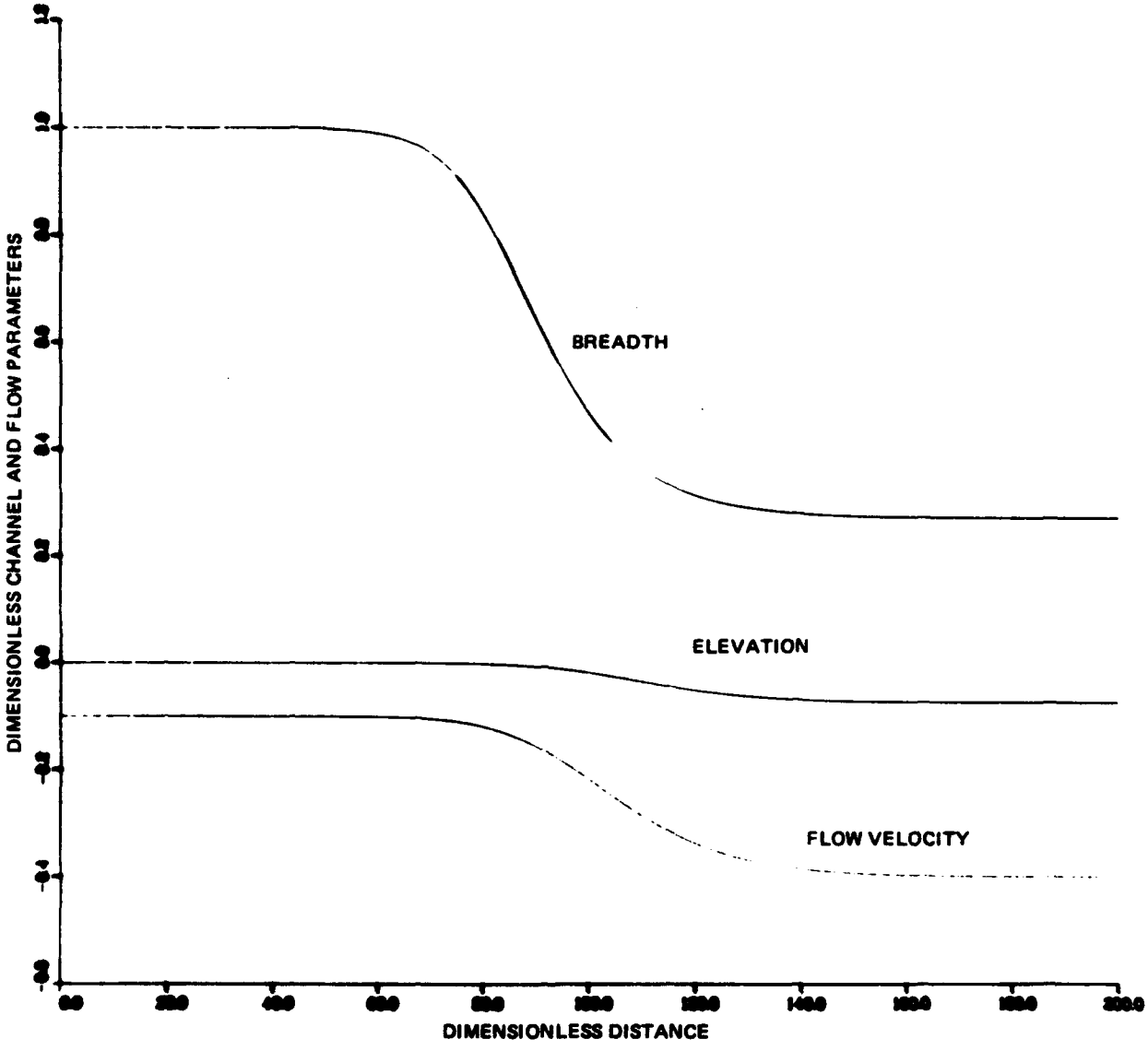

Fig. 3 — Geometry and steady flow conditions for the computations of Fig. 2